https://doi.org/10.5194/egusphere-2025-2889
Preprint. Discussion started: 15 August 2025

# EC-Earth- and ERA5-driven ensemble hindcasts with the fully coupled ice-sheet–ocean–sea ice–atmosphere–land circum-Antarctic model PARASO

Florian Sauerland[1,*], Pierre-Vincent Huot[1,*], Sylvain Marchi[1,2], Thierry Fichefet[3], Hugues Goosse[3], Konstanze Haubner[4,5], François Klein[3], François Massonnet[3], Bianca Mezzina[3,6], Eduardo Moreno-Chamarro[7], Pablo Ortega[7], Frank Pattyn[4], Charles Pelletier[3,6], Deborah Verfaillie[3,8], Lars Zipf[4], and Nicole van Lipzig[1]

[1]Department of Earth and Environmental Sciences, KU Leuven, Leuven, Belgium
[2]Royal Meteorological Institute of Belgium, Climate Modeling and Impact studies, Brussels, Belgium
[3]Earth and Life Institute, UCLouvain, Louvain-la-Neuve, Belgium
[4]Laboratoire de Glaciologie, ULB, Brussels, Belgium
[5]Department of Earth Science, University of Bergen, Bjerknes Centre for Climate Research, Bergen, Norway
[6]European Centre for Medium-range Weather Forecasts (ECMWF), Bonn, Germany
[7]Barcelona Supercomputing Center (BSC), Barcelona, Spain
[8]Aix Marseille University, CNRS, IRD, INRAE, CEREGE, Aix-en-Provence, France
[*]These authors contributed equally to this work.

**Correspondence:** Florian Sauerland (florian.sauerland@kuleuven.be)

**Abstract.** The origins of recent and ongoing Antarctic climate trends are topic of debate, partly because trends and variability can originate from both the Antarctic climate system itself as well as from the mid-latitudes. Furthermore, we lack observations for a detailed analysis of these effects. Here, we use the regional ice sheet–ocean–sea ice–atmosphere–land circum-Antarctic model PARASO to produce four hindcasts of the Antarctic climate over the 1985-2014 period. The first is a control simulation, forced by atmospheric and oceanic reanalyses (ERA5 and ORAS5), realistically reproduces the pre-2017 increase in Antarctic Sea Ice Extent (SIE) and Surface Mass Balance (SMB) of the Antarctic Ice Sheet. In contrast, the other three hindcasts, driven by EC-Earth historical simulations, simulate a declining SIE and increasing SMB over the same period, a behaviour consistent with biases seen in many global climate models, suggesting that biases in these models may be due to misrepresented lower-latitude dynamics or poleward transports. While both ERA5- and EC-Earth-driven simulations reproduce a dipole in sea ice concentration trends—positive in the east and negative in the west—the magnitude differs. The larger negative trend in the West in the EC-Earth-driven simulations feature a stronger intensification and displaced Amundsen Sea Low, enhancing northerly winds, moisture and heat flux between the Ross and Amundsen Sea. In turn, the different trends in SIE between the ERA5 driven and EC-Earth driven hindcasts result in opposing trends for moisture transport towards Antarctica and precipitation. By comparing the agreement between the three EC-Earth driven hindcasts, a small imprint of internal climate variability was found over the Southern Ocean, whereas this imprint over the continent is much stronger. Nonetheless, all EC-Earth driven simulations exhibit a robust positive SMB trend, indicating a link with sea ice decline or with large-scale advection shared across ensemble members.

https://doi.org/10.5194/egusphere-2025-2889
Preprint. Discussion started: 15 August 2025

## 1 Introduction

The evolution of the Antarctic climate over the past decades has raised many questions about how it has responded and will respond to anthropogenic global warming. In the Arctic, near-surface air warming has been up to four times faster than in the rest of the world due to polar amplification (Goosse et al., 2018; Rantanen et al., 2022), but the same effect cannot be detected over Antarctica (Wang et al., 2016; Jones et al., 2019; Turner et al., 2020). The Antarctic sea ice extent (SIE) had a slightly positive trend before 2017 (Parkinson, 2019), seemingly inconsistent with the observed global temperature increases. This trend was only locally significant (Yuan et al., 2017) though, and after 2017, SIE has remained in a persisting low state. At the same time, some signals stand out from natural variability: westerly winds are strengthening and shifting poleward, and West Antarctica and the Antarctic peninsula are warming (Jones et al., 2019). While some of these signals are captured and confirmed by theoretical findings, even the last generation of global climate models – which are also the tools used to forecast the future of the Antarctic climate – fail to reproduce most of the observed changes (Roach et al., 2020; Heuzé, 2021). Simulated long-term trends for sea ice extent match better with the more recent decrease in sea ice (Holmes et al., 2024), however. This questions the ability of such models to forecast the evolution of the Antarctic climate and challenges the origin of the observed changes: which signals are actually imputable to the anthropogenic forcing and which ones resort from internal climate variability? Internal variability has been invoked multiple times to explain the current changes (Turner et al., 2015, 2016; Singh et al., 2019). And indeed, due to the short temporal and limited spatial coverage of observations in Antarctica and the Southern Ocean, it is difficult to estimate the role of natural variability in Antarctic climate variability, which in turn complicates attributing observed changes to global warming over pluri-annual to decadal time scales. Answering these questions is essential for reliable Antarctic climate projections, at a moment when the Antarctic system could, or has already reached profound transitions (Favier et al., 2014; De Lavergne et al., 2014; Kittel et al., 2021).

A common practice to estimate the contribution of internal variability to observed changes is to conduct ensemble simulations with global climate models (GCMs). But the reliability of GCMs for the representation of the Antarctic climate can indeed be questioned. Climatic conditions of polar regions are so different from other parts of the globe that both the sets of parameters as well as some of the parameterizations themselves are unlikely to be suitable for polar applications. They are optimized to minimize the mismatch between the observed and simulated climate of the Earth, without focusing only on Antarctica. Even with the desire to adapt these parameters to the climate of Antarctica, large observational uncertainties limit the development of satisfactory parameterizations. In general, polar regions are the scene of many processes involving the cryosphere, such as glacier flow, floating ice shelves interacting with the ocean, iceberg drift, sea water freezing, as well as strong surface inversions, katabatic winds, and many more, which in many models are poorly implemented or even fully absent. Observational studies and models specifically designed for polar regions on the other hand have illustrated the key role of such processes in shaping the Antarctic climate and its connection to the Earth's climate (e.g., De Lavergne et al., 2014; Donat-Magnin et al., 2017; Huot et al., 2021). Too low resolution, limited understanding and missing technical developments are preventing GCMs (and models in general) to accurately reproduce the channeling of coastal katabatic winds and formation of polynyas, the open ice shelves cavities including their ocean circulation, the spatial patterns and variability of surface and basal mass balance of the Antarctic Ice Sheet and the associated migration of ice shelves grounding lines. Regional climate models specifically designed to represent the Antarctic climate and taking into account the specific processes of polar regions are now able to simulate the Antarctic climate more realistically (e.g., Barrand et al., 2013; Mottram et al., 2020). A remaining central difficulty is the necessity of representing these interactions between different components of the climate system taking place on a wide range of temporal (seconds to centuries) and spatial (100s of meters to global) scales. Most regional models only account for one or two of those components (e.g. atmosphere-land, ocean-sea ice, ocean-ice sheet). At the interface between earth system modeling and regional climate modeling, the regional circum-Antarctic ocean–sea ice–atmosphere–ice sheet–land model PARASO has been developed by Pelletier et al. (2022) (hereafter P22). It reproduces the Antarctic climate and its subcomponents more realistically than GCMs while retaining their ability to study both the forced response and internally generated long-term (interannual to decadal) variability. A key novelty in PARASO is the asynchronous coupling allowing for the required different time steps of atmosphere (seconds), ocean and sea-ice (minutes) and ice sheet (daily/weekly).

In this paper, the role of low latitudes (north of 60°S) in the regional Antarctic climate trends over the period 1985 – 2014 is studied. Moreover, the role of the internal climatic variability on the one hand and the role of forced response due to greenhouse gases on the other hand is investigated. For this purpose, we created a total of four hindcasts with PARASO: a hindcast forced with ERA5 and ORAS5 reanalysis data at the boundary and initial conditions, and a small ensemble of three hindcasts using EC-Earth GCM hindcasts for their boundary and initial conditions. The three EC-Earth driven hindcasts are each initialized using slightly perturbed conditions, but use boundary conditions dervied from three independent EC-Earth hindcasts where the initial conditions were also perturbed. We assess the roles of internal variability, external forcing due to greenhouse gases, and predictable signals by comparing the trajectories of the three EC-Earth driven hindcasts. Furthermore, we identify the differences in model trajectories when driving the regional model at lateral boundaries using ERA5 against EC-Earth. The EC-Earth driven hindcasts are designed to represent a set of trajectories that are compatible with the GCM's initial and boundary conditions, but that may not be representative of the actual state of the climate system due to different timing of the natural variability.

First, the capabilities of PARASO to simulate the Antarctic climate is investigated on decadal timescales, extending the study of P22. In particular, this analysis sheds light on the longstanding discussion of whether the decreasing sea ice extent, contradicting the observations before 2014, generally simulated by GCMs is due to their misrepresentation of polar processes in the Southern Ocean and Antarctica or if it is related to the coupling with lower latitudes. Moreover, we analyze the impact of changes in temperature and moisture advection in the boundary conditions on the sea ice, as well as that of atmospheric circulation patterns. Particular focus is given on the interconnections of the moisture balance of the region, consisting of moisture transport from mid-latitudes, precipitation and evaporation over the ocean and sea ice, moisture transport to the continent, and precipitation and evaporation over the continent. Finally, the linkages between the moisture balance terms, temperature, atmospheric circulation, and cloud properties are examined.

https://doi.org/10.5194/egusphere-2025-2889
Preprint. Discussion started: 15 August 2025

## 2 PARASO hindcasts

We conducted a total of four 30-year long hindcasts: a control experiment forced by atmospheric (ERA5, Hersbach et al., 2020) and oceanic (ORAS5, Zuo et al., 2019) reanalyses over the 1985-2021 period, named ERA-5 driven (E5D) hindcast in the following, and a three-member ensemble forced by three global hindcasts produced by the EC-Earth global coupled model (Döscher et al., 2022) over the 1985-2014 period, with the individual ensemble members named FC00, FC01, and FC02. The model employed for this study is briefly described in Sect. 2.1. Details on the setup of the ensemble can be found in Sect. 2.2 to 2.4, which includes Sect. 2.3 about the global EC-Earth hindcasts used for the forcing at the lateral boundaries and for deriving the initial conditions.

### 2.1 The PARASO model

The model used in this study is referred to as PARASO. Since a full technical description is available in P22, including a corrigendum that has been taken into account for this study, here we only describe its main features. It has already been proven to be useful to study physical processes in the Southern Ocean (Mezzina et al., 2024). PARASO is a fully-coupled five-model configuration covering the full Antarctic continent and surrounding Southern Ocean, running at a horizontal resolution of about $0.25°$ ($\approx$ $8\mathrm{km}$ at the Antarctic coastline for the ocean). The models used for each Earth system subcomponents are f.ETISh1.7 for the Antarctic ice sheet (Pattyn, 2017; Coulon et al., 2021), NEMO3.6 (Madec, 2016) for the free ocean, LIM3.6 for the sea ice (Vancoppenolle et al., 2009; Rousset et al., 2015), COSMO5.0 for the atmosphere (Rockel et al., 2008), and CLM4.5 (Oleson et al., 2013) for the ice sheet and grounded snow surfaces. All of these models are state-of-the-art and have been used in CMIP6-type (Eyring et al., 2016) experiments.

The COSMO-CLM (atmosphere and land, hereinafter CCLM$^2$) model configuration is derived from Souverijns et al. (2019), with a few modifications such as enhanced vertical resolution, domain coverage increase, and modification in the snow scheme. The NEMO configuration is primarily based on GO7 from Storkey et al. (2018), and the LIM configuration from Rousset et al. (2015) and Barthélemy et al. (2018). The combination of these last two models is referred to as NEMO-LIM. The coupling between CCLM$^2$ and NEMO-LIM is carried out online (i.e., while each model runs) through the OASIS3-MCT coupler (Valcke, 2013). For the land ice-ocean interaction in PARASO, NEMO (ocean) and f.ETISh (ice) are coupled offline. The geometry of the Antarctic Ice Sheet (AIS) evolves in time to react to ice-shelf basal melt in NEMO (computed through explicitly simulated ice-shelf cavities, see Mathiot et al., 2017), and these geometry changes are then accounted for in NEMO (Smith et al., 2021). PARASO also includes a one-way coupling from CCLM$^2$ (atmosphere-land) to f.ETISh (ice sheet) by providing the surface mass balance (SMB) over the ice area. In our setup however, the changes of the ice surface during the 30yr simulation period are negligible and we keep therefore the initial ice surface within COSMO. All modifications from the references given above are thoroughly described in Section 2 and 3 of P22.

https://doi.org/10.5194/egusphere-2025-2889
Preprint. Discussion started: 15 August 2025

### 2.2 Forcing

The first PARASO hindcast uses reanalysis data as its lateral forcings. For this reanalyses-driven simulation, ERA5 data is used for the atmosphere forcings and ORAS5 data for the ocean forcings. Forcing is applied at the lateral boundary of the ocean, at the surface of the ocean outside the coupled domain, and at the lateral boundaries of the COSMO domain (see Fig. 3a for an overview of the domain). There is no additional nudging towards the GCM or reanalysis solution within the coupled domain in order to let weather system develop freely within the regional model domain. The forcing procedure is described in detail in P22. The only differences with respect to P22 regarding the forcing are the addition of a 10 grid-point transition zone between forced and coupled domain at the imprint of the COSMO boundary onto the NEMO grid, and the forcing frequency when using the EC-Earth forcing (6 hours instead of 3 hours when using ERA5).

The other three EC-Earth-driven PARASO hindcasts are forced by atmospheric (Integrated Forecasting System of the European Centre for Medium-Range Weather Forecasts, IFS) and oceanic (Nucleus for European Modelling of the Ocean, NEMO) outputs from three global EC-Earth hindcasts which are described in section 2.3. To limit the risk of inheriting biases from the EC-Earth boundary conditions, these have been bias corrected. For the ocean, monthly biases between EC-Earth and ORAS5 were removed from oceanic temperature and salinity. For the atmosphere, the climatological (seasonally varying, monthly frequency, then interpolated to daily) bias between EC-Earth and ERA5 was removed from temperature and specific humidity. The strength of the bias correction decreases with height, starting from 100% near the surface, and then decreases to 0% at the first local minimum in temperature. This is motivated by the facts that ERA5 is less constrained in the stratosphere and thus likely less realistic than in the troposphere, that EC-Earth biases are smaller higher up in the troposphere, that lower-troposphere heat and moisture are most important to represent the hydrological cycle correctly in the regional model, and to avoid displacing the tropopause by applying the bias correction. The mean temperature and specific humidity biases of EC-Earth with respect to ERA5, together with an illustration of the depth-dependence of the bias-correction are shown in Figure A1.

### 2.3 EC-Earth simulations

The three global hindcasts used to force the PARASO hindcasts ensemble were produced using the EC-Earth GCM version 3.3. This is the official version contributing to CMIP6, whose configuration and main characteristics are described in detail in Döscher et al. (2021). It incorporates the ECMWF's IFS global atmosphere–land model, cycle 36r4, the NEMO3.6 global ocean model with the LIM3 sea ice module, and the OASIS3-MCT coupler. The IFS model uses a T255 spectral resolution and has 91 vertical levels up to 0.01 hPa. The NEMO model uses the ORCA1 tripolar grid, which has a horizontal resolution of about 1°, and has 75 vertical levels. LIM3 is a dynamic–thermodynamic sea-ice model with five ice thickness categories.

To produce the initial conditions for the EC-Earth hindcasts, we first generate a reconstruction for the period 1980 — 1985. The atmosphere uses full-field nudging toward ERA-Interim in temperature, surface pressure, vorticity, and divergence, as in Kröger et al. (2018). The relaxation timescale is 1-hourly, which is of moderate strength. The ocean uses anomaly nudging toward ORAS4 temperature and salinity, similar to Volpi et al. (2017). We use anomaly initialization in the ocean to avoid the presence of forecast drifts, which would need a full set of retrospective predictions to be properly diagnosed and corrected. This method has also helped us to avoid an initialization shock that affects the full field initialized decadal predictions performed with EC-Earth, in which Labrador Sea convection experiences a rapid collapse (Bilbao et al., 2021).

To produce the ORAS4 anomalies, we replace the ORAS4 climatology for the period 1980–2014 by one computed from the ensemble mean of 10 CMIP6 historical simulations that are generated with the same EC-Earth model version. The subsurface nudging relaxation timescale is relatively weak: 30 days and 3600 days above and below 800 m respectively. At the surface, the model is restored in temperature and salinity, with a damping magnitude equal to –40 $\mathrm{Wm^{-2}K^{-1}}$ and –166.67 $\mathrm{kg\,m^{-2}s^{-1}psu^{-1}}$ respectively. All three reconstructions start on 1 January 1980, branching off from the second member (r2i1p1f1) of the CMIP6 historical ensemble of EC-Earth (also included in the ensemble mean of the 10 members mentioned above). The reconstructions use CMIP6 historical forcings, as in the free-running historical simulations. Each reconstruction assimilate a different member of ORAS4. The reconstructions provide the initial conditions for the three hindcasts used for the PARASO boundary and initial conditions. These start on 1 November 1984, as in the CMIP6 DCPP protocol (Bilbao et al., 2021), and run for 30 years until 1 November 2014. These hindcasts are global EC-Earth free runs (i.e., no nudging toward observations) and also use the external forcing from CMIP6.

### 2.4 Initialization

The initialization of a regional coupled model involving components evolving on such a large variety of time scales (from seconds to centuries) is a delicate task, and no consensus currently exists on what are the best practices. In our case, the goal of the initialization is multiple, as it should limit initial shocks, generate a realistic initial state that accounts for observed uncertainties, as it might be a source of predictability, and generate the ensemble spread.

#### 2.4.1 CCLM$^2$

For the timescales considered in this study (seasonal to interannual), knowledge about the atmosphere's initial state will likely not provide any insights into the evolution of the Antarctic climate. For the EC-Earth-driven hindcasts, COSMO's initial states are derived from EC-Earth hindcasts on the 1st of January 1985, following the bias-correction procedure described earlier. Accordingly, the initial atmospheric state differs from one member to the other, but consistency between the initial state and the lateral forcing is preserved avoiding initial shocks. As the snow cover takes longer to reach equilibrium, the snow mantle (and land in general) is initialized using a CLM restart from a previous coupled experiment. All members start from the same land and snow state.

#### 2.4.2 f.ETISh

Initializing f.ETISh is challenging, as the Antarctic Ice Sheet takes centuries or even millennia to adjust to its forcing in coupled mode (if such equilibrium can be defined in a perpetually evolving climate), and the coupled ocean-ice sheet model cannot be run for such long periods. Here, we use the initial ice sheet state produced by the two steps procedure of P22. During the first step, a simplified version of f.ETISh with fixed observed ice shelves is run for 60 kyr with basal melt obtained from a NEMO standalone run and SMB derived from the COSMO run presented in Souverijns et al. (2019). During this run, basal stress is iteratively adjusted to produce an ice sheet geometry and velocity field matching the observed ones. Then, a 20-yr relaxation run is performed with f.ETISH using the full complexity and evolving ice shelf geometry. In the end, the Antarctic Ice Sheet is balanced with the buttressing of the observed ice shelves, and the ice shelves' geometry is at least partially adapted to the simulated Antarctic Ice Sheet velocity field.

### 2.4.3 NEMO-LIM

The ocean is another potential source of long-term predictability. The ocean and sea ice initial states in the ERA5-driven hindcast were produced by a standalone one-year NEMO-LIM simulation with the ERA5 forcing of the year 1984, taken at the end of the simulation. This standalone NEMO-LIM spin-up run was itself initialized from the standalone NEMO-LIM climatology used to build the initialization of the EC-Earth driven hindcasts: In the EC-Earth driven hindcasts, we initialize the ocean from a climatological restart (mean of 20 oceanic restarts for the 1st of January between 1990 and 2010) of a standalone NEMO-LIM run forced by ERA5 to minimize initial model shock and drift. This also presents the advantage of starting from an ocean that is not at rest. To produce a realistic initial state (i.e., with initial anomalies representative of a particular year, instead of a climatological state which would otherwise provide no initial information), and to keep the consistency with the EC-Earth hindcasts, the ORAS4 anomalies for the 1st of January 1985 (with respect to the ORAS4 climatology) were added to this ocean climatology. For consistency, we use the same ORAS4 members as the ones used to build the set of EC-Earth hindcasts' initial states. The differences between the temperature and salinity anomalies of the three members are small in comparison to the magnitude of the anomalies (Fig. A2), meaning that the three hindcasts start with quasi-identical initial states (averaged root-mean-square deviation between the members' initial states of 0.09 K for temperature and 0.01 g per kg for salinity over the first 1000 m). The initial spread represents the observational uncertainties about the oceanic conditions on the 1st of January 1985, as estimated from the ORAS4 reanalysis. For the sea ice, we use the raw climatological restarts (spatially varying sea ice concentration, thickness, and snow cover) of a NEMO-LIM standalone run which is identical for the three runs.

## 3 Model evaluation

A first evaluation of the model including some sensitivity experiments to model parameters was conducted in P22. However, this evaluation relied on short-term (two year) simulations. Here, we extend this evaluation to 30-year-long simulations, allowing us to test the long-term stability of the coupled model and the realism of EC-Earth-driven hindcasts. Overall, the 30-year long runs presented here compare well with standalone experiments (not shown, see P22), indicating that the coupling does not degrade the simulated mean state on longer timescales. Ocean temperatures agree well with observations for both forcings (i.e. EC-Earth and ERA5/ORAS5), although a 1 to 2 K cold bias can be found in the coastal areas of the Amundsen and Bellinghausen Seas below 250 m (see Fig. A3b and c), as well as biases in the upper ocean above 100m in the open ocean of the Bellinghausen Sea (2 K cold bias in the ERA5 driven simulation, 1 K cold biases in the EC-Earth driven simulations, Fig. A3c), and biases in the Western Pacific (warm bias of approximately 1 K in the upper ocean, Fig. A3f)

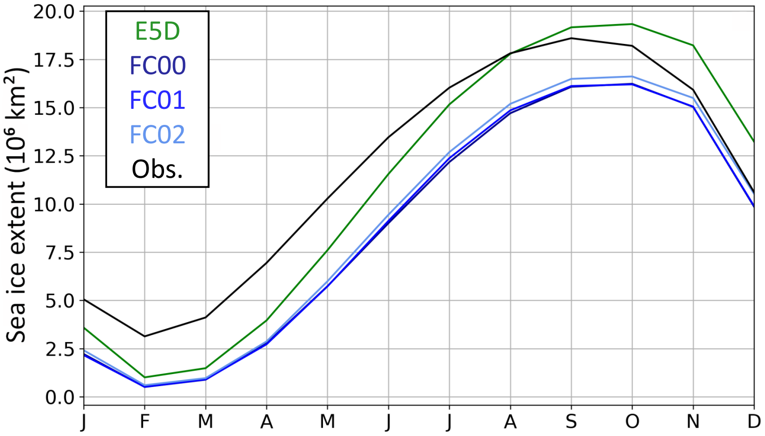

**Figure 1.** Mean Antarctic Sea Ice Extent seasonal cycle simulated in the ERA5-driven hindcast (E5D), the three EC-Earth-driven hindcasts (FC00 – FC02), and observed in the OSI-409 dataset.

The mean seasonal cycles of sea ice extent (SIE) simulated by the four PARASO hindcasts are presented and compared with observations in Figure 1. All four experiments simulate a lower than observed summer SIE, with a mean bias of $3.20 \cdot 10^6$ km$^2$ in the EC-Earth-driven ensemble and $2.63 \cdot 10^6$ km$^2$ in the ERA5-driven run. Summer SIE in standalone ocean-sea ice configuration (see P22) also shows a negative summer SIE bias, which is here likely amplified by the coupling with the atmosphere. The winter SIE maximum is delayed by one month and slightly overestimated in the ERA5-driven run ($0.56 \cdot 10^6$ km$^2$, Fig 1) while being underestimated in the EC-Earth-driven runs (by $-2.37 \cdot 10^6$ km$^2$ on average). The influence of the lateral forcing is visible here, with an RMSE of $2.00 \cdot 10^6$ km$^2$ for the (more observationally restricted) ERA5-driven run and and $3.14 \cdot 10^6$ km$^2$ for the EC-Earth-driven ensemble. Nevertheless, the amplitude of the seasonal cycle is correctly captured by the EC-Earth-driven experiments, while being overestimated in the ERA5-driven one.

Temperature and wind speed are on average well represented in PARASO. All simulations have a cold bias of about 2 K over the AIS in their 2m temperature compared to ERA5, except for some warm peaks over the Transantarctic Mountains (Fig. 2a), which is likely the result of a different orographic roughness length, leading to more turbulent exchange with air higher up in PARASO than in ERA5. Over the ocean, the EC-Earth driven hindcasts have a near-universal warm bias, agreeing with the underestimated sea ice concentration. The warm bias does not have the same extent in the ERA5-driven hindcast, where it is only warmer than ERA5 in East Antarctica and in the Ross Sea, in agreement with the findings from P22. For the 10m wind speed, the largest differences can once again be found over the Transantarctic Mountains for all models (Fig. 2b), where PARASO simulates a much higher wind speed than ERA5, most likely again caused by the different implementation of subgrid-scale orography (P22). Over the Antarctic Continent, no other clear pattern can be observed, over the Southern Ocean on the

https://doi.org/10.5194/egusphere-2025-2889
Preprint. Discussion started: 15 August 2025

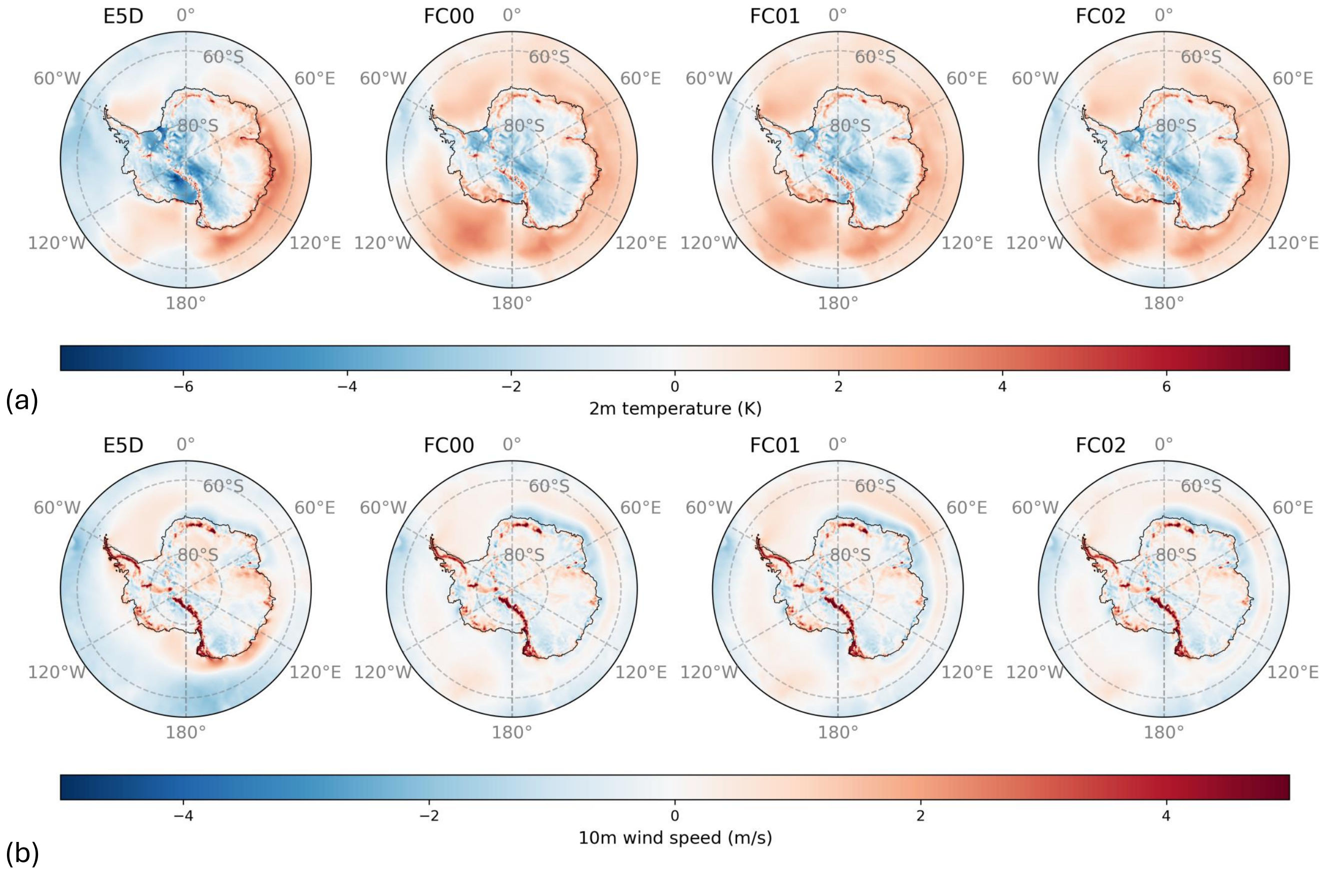

**Figure 2.** The 30 year average bias (PARASO - ERA5), in 2m temperature (a) and 10m wind speed (b), for the ERA5-driven hindcast (E5D) and the three EC-Earth-driven hindcasts (FC00 – FC02).

other hand, the ERA5-driven hindcast underestimates wind speeds compared to ERA5 for most of the Western Hemisphere, in the Amundsen, Bellinghausen and Ross Seas, whereas the EC-Earth driven hindcasts slightly overestimate wind speed in the same areas. This pattern inverts in the coastal seas, especially close to the Ross Ice Shelf, where the ERA5-driven hindcasts overestimates wind and the EC-Earth driven hindcasts underestimate it. In the Eastern Hemisphere, the two different forcings mostly agree, with a slight underestimation along the coasts quadrant closer to the Greenwich Meridian, which turns into a slight overestimation further off the coast, and the inverse of this coast/high sea pattern in the other quadrant.

## 4 Results

In this section, we present the simulated long-term trends and how they differ between ERA5 and EC-Earth driven runs, as well as in between the ensemble members of the EC-Earth driven runs. Through the first comparison, we estimate the influences of the different lateral boundary conditions and initial conditions, while the second comparison allows us to get a measure

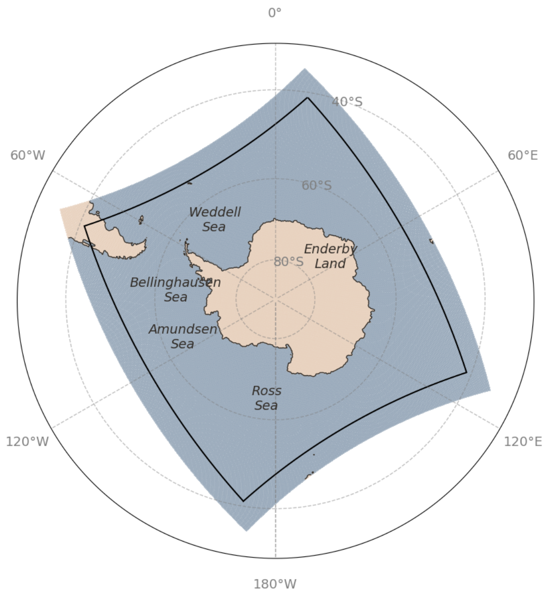

**Figure 3.** An overview of the model domain and used region denominations in this paper. The areas considered a land area are indicated in brown, i.e. shelf ice is considered as part of the land area for atmospheric variables. The southern part of South America, as well as the Falkland and South Sandwich Islands are included the COSMO model domain, but do not form part of the Antarctic continent, therefore they are excluded from the evaluations unless otherwise specified. The extent of the plot (i.e., everything south of 30°S) is part of the NEMO domain. The COSMO domain is composed of the colored areas which feature the land/sea mask shown. Overlayed on the COSMO domain is a black rectangle, this is the evaluation domain.

of internal variability. Since all EC-Earth driven experiments share quasi-identical initial states, all of those simulations are affected by similar forcing signals (due to greenhouse gases etc.) and model drift, while the timing of the internal variability may vary. Differences in long-term trends should therefore be the result of internal climate variability, generated outside and/or inside the domain.

Unless otherwise specified, the trends mentioned are evaluated over the COSMO domain. In addition to the 10 gridpoint relaxation zone where the lateral forcings are imprinted on the model results, we add a 12 gridpoint buffer zone that we leave out of our evaluation, so that in total 22 gridpoints at all lateral boundaries are cut out of our evaluation domain (see Fig. 3). Furthermore, and unless otherwise specified, we calculated the trends by using seasonally detrended monthly averages and applying the Mann-Kendall test to determine the trends' significances. Antarctica/domain-wide trends are also weighted by area to account for differently sized grid cells.

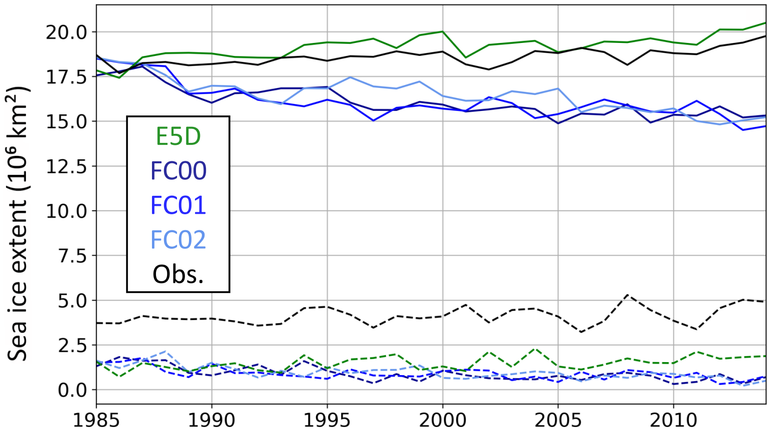

**Figure 4.** Time series of September (solid line) and March (dashed line) sea ice extent, as simulated by the three EC-Earth-driven hindcasts (FC00 – FC02), the ERA5-driven hindcast (E5D), and as observed in the OSI-409 dataset (EUMETSAT, 2015).

### 4.1 Sea ice

One of the most puzzling aspects of the recent Antarctic climate evolution is the increase, or at least, the absence of a decrease in the Antarctic Sea Ice Extent (SIE) prior to 2014. Over the 1985-2014 period, the observations from the OSI-409 dataset (EUMETSAT, 2015) indeed suggest a September SIE increase, with a trend of $0.34 \cdot 10^6$ km$^2$ per decade, while March SIE remains stable (Fig. 4). The ERA5-driven hindcast is reproducing the observed increase in September SIE (Fig. 4), slightly overestimating the observed trend at $0.57 \cdot 10^6$ km$^2$ per decade (Tab. 1). The ability of PARASO to reproduce the observed SIE trend when being forced by observationally constrained reanalyses demonstrates its usefulness and added value compared to existing tools, as most GCMs fail to simulate this feature (Roach et al., 2020). On the other hand, the EC-Earth-driven hindcasts are all simulating a significant negative September SIE trend, averaging at $-0.87 \cdot 10^6$ km$^2$ per decade with low member-to-member variability, hence reproducing the typical behavior of most GCMs. The fact that PARASO reproduces the negative trend commonly simulated by GCMs when forced by such models suggests the importance of conditions imposed from the midlatitudes in setting the Antarctic SIE pluri-decadal trends. This implies that the differences in the representation of physical processes at high southern latitudes do not explain the opposite SIE trends as the ERA5-driven and EC-Earth-driven hindcasts share the same model configuration and only differ in their forcing. In turn, this suggests a weaker role of the misrepresentation of polar processes, sometimes advanced to explain the biases of GCMs. The EC-Earth hindcasts themselves are not showing a negative SIE trend (Mann-Kendall test for the ensemble averaged September SIE: p = 0.972, March SIE: p = 0.475), but they simulate a much smaller winter SIE (Ensemble mean for September SIE over the simulation period: $10.27 \cdot 10^6$ km$^2$) than simulated in the EC-Earth driven PARASO hindcast. As the EC-Earth simulations were free running after 1985, this shows that the simulated trends in the EC-Earth driven PARASO hindcasts are not originating from a model drift intrinsic to EC-Earth. The differences in SIE trend must therefore originate from differences in the lateral forcing such as for instance different warming in ERA5 and EC-Earth, which we analyze in Sec. 4.2. The incomplete deep ocean and ice sheet spin-up

https://doi.org/10.5194/egusphere-2025-2889
Preprint. Discussion started: 15 August 2025

| | **SIE September** ($10^6$ km$^2$/10yr) | **SIE March** ($10^6$ km$^2$/10yr) |
|---|---|---|
| E5D | 0.50 | 0.21 |
| FC00 | $-0.79$ | $-0.32$ |
| FC01 | $-0.77$ | $-0.23$ |
| FC02 | $-1.00$ | $-0.30$ |

**Table 1.** Decadal trends computed over 1985-2014 for the ERA5-driven hindcast (E5D) and the three EC-Earth-driven hindcasts (FC00 – FC02). SIE: Sea ice extent. All trends were statistically significant ($p < 0.05$).

cannot be ruled out as a source of long-term adjustment, but their influence on surface ocean properties and sea ice should be limited compared to atmospheric forcing after a few years of simulation. In addition, the initial ocean and ice sheet states used 275 for the ERA5-driven and EC-Earth-driven hindcasts are very similar (for the ocean) or identical (for the ice sheet). The fact that all three EC-Earth-driven hindcasts simulate almost the same negative SIE trend suggests that internal variability only plays a limited role.

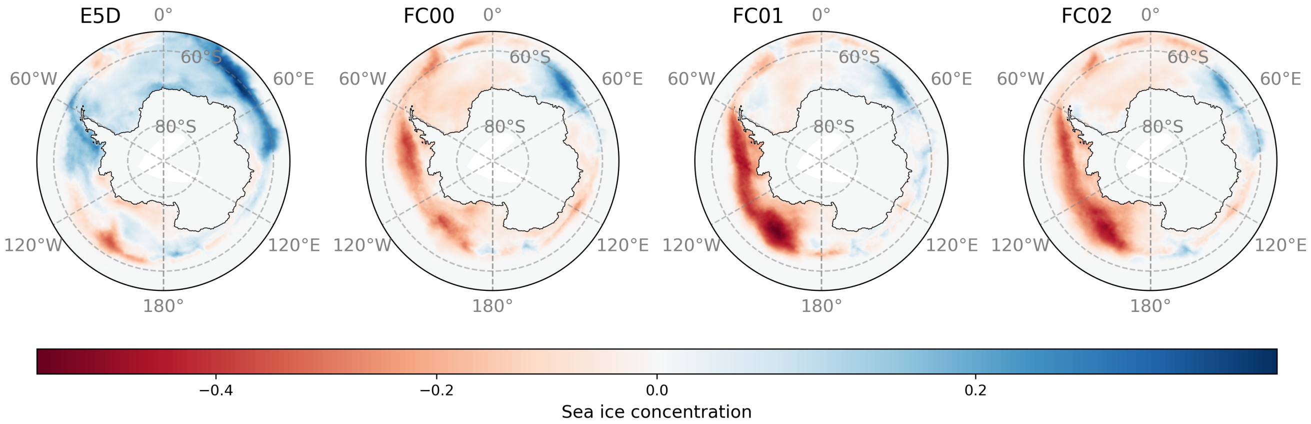

**Figure 5.** Change of sea ice concentration in the 2009–2014 average, compared to the 1985–1990 average, all seasons, for the ERA5-driven hindcast (E5D) and the three EC-Earth-driven hindcasts (FC00 – FC02). Averages are used in this figure because trends computed using a linear fit per grid cell are not statistically sound (sea ice concentration cannot go lower than zero or higher than one, and therefore even a significant trend would be capped off and turn to a flat one).

The changes in sea ice concentration during the simulated period are not distributed homogeneously around the continent: in the eastern part of the Southern Ocean, the sea ice concentration has generally increased, while there is a decrease in sea 280 ice concentration in the western part, particularly in the Amundsen Sea, both for the ERA5 driven and the hindcast driven runs (Fig. 5). The area with a sea ice increase is much larger in the ERA5 driven run and also encompasses the Antarctic Peninsula, which shows a sea ice decrease in the EC-Earth driven runs. The decrease in sea ice in the Amundsen Sea is expected, with stratospheric ozone depletion resulting in an intensification of the Amundsen Sea Low (Dalaiden et al., 2022). More surprising is the increase in sea ice extent in East Antarctica, which is consistently simulated in all models.

### 4.2 Temperature, wind, and geopotential

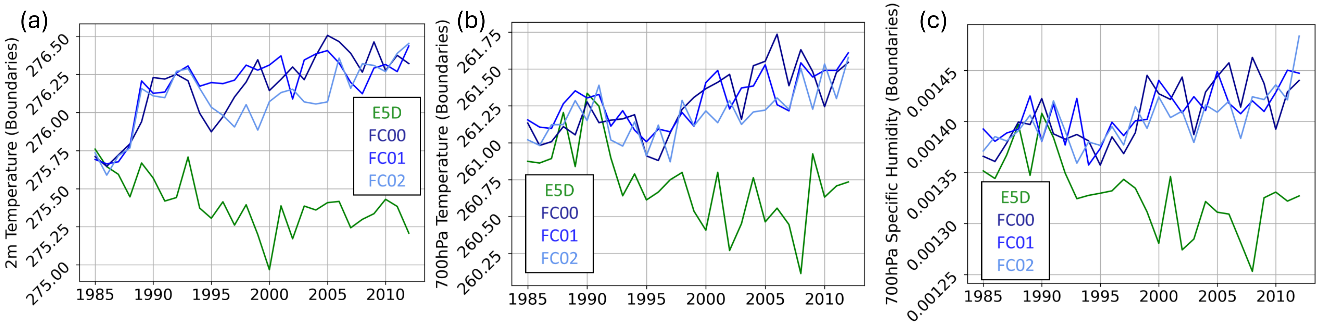

**Figure 6.** 2m temperature in K (a), 700hPa temperature in K (b) and 700hPa specific humidity in kg per kg (c) averaged along the evaluation domain boundary in the ERA5-driven hindcast (E5D) and the three EC-Earth-driven hindcasts (FC00 – FC02).

To identify the role of potentially different rates of warming applied at the boundaries of the regional model from ERA5 or EC-Earth, we compare the yearly-averaged variations of air temperature and specific humidity, averaged along the evaluation domain boundary (the outermost gridcells of the evaluation domain and the innermost gridcells of the bufferzone), simulated by the ERA5 driven and EC-Earth driven hindcasts (Fig. 6). At 700 hPa, the ERA5-driven hindcast is simulating a 0.18 K per decade cooling trend, which is also persistent in the 2m temperatures (0.11 K per decade). The 700 hPa temperature seems to recover from 2009 onwards for the ERA-5 driven run, but it is too close to the end of our simulation to test if it is a new trend or the result of short-term variability. Specific humidity is showing a similar evolution with a 0.026 $\mathrm{g \cdot kg^{-1}}$ per decade drying trend, which would be expected from the Clausius-Clapeyron relationship. EC-Earth-driven hindcasts on the other hand are simulating a 700 hPa warming at the boundaries ranging between 0.14 and 0.21 K per decade and a moistening trend between 0.020 and 0.026 g per kg per decade. Through this opposite trend, the temperatures in the ERA-5 driven hindcast drop below the temperatures in the EC-Earth driven hindcasts: Initially, the 700hPa temperature at the boundaries is around 261K (-12°C) for all hindcasts, at the end of the simulation period, the EC-Earth driven hindcasts simulate a temperature around 1K warmer than the ERA-5 driven one. It is also worth noting that all of the EC-Earth driven simulations simulate a cooler period in their 700hPa temperatures between 1991 and 2000, superposed onto the long-term warming trend, suggesting that this cooler period has the potential to be predicted up to 5 years in advance.

In the ERA5 driven hindcast, the cooling observed at the lateral boundaries extends over the Southern Ocean, where the model simulates a cooling trend of 0.11 K per decade at a 2m height (Tab. 2) and a cooling trend of 0.15 K per decade at 700 hPa. In general, the 2m and 700hPa temperature trend agree in direction and significance, though their magnitude can vary slightly. This cooling trend is consistent with the SIE increase seen in the ERA5-driven hindcast as was, for instance,

| | **T 2 m SO** (K/10 yr) | **T 700 hPa SO** (K/10 yr) | **T 2 m AA** (K/10 yr) | **Westerlies 51°S – 58°S** (m/s/10yr) | **Easterlies 66°S – 70°S** (m/s/10yr) |
|---|---|---|---|---|---|
| E5D | −0.11 | −0.15 | −0.07* | 0.045* | −0.023* |
| FC00 | 0.31 | 0.24 | 0.27 | 0.200 | −0.025* |
| FC01 | 0.28 | 0.20 | 0.23 | 0.026* | −0.008* |
| FC02 | 0.30 | 0.16 | 0.14* | 0.083* | 0.027* |

**Table 2.** Decadal temperature and wind trends computed over 1985-2014 for the ERA5-driven hindcast (E5D) and the three EC-Earth-driven hindcasts (FC00 – FC02). An asterisk indicates an insignificant trend ($p > 0.05$). T 2m SO: 2 m air temperature over the Southern Ocean and sea ice (within the evaluation domain), T 2m AA: 2 m air temperature over Antarctica, Westerlies: average 10 m westerly winds strength (counted positive eastward) taken between 51 and 58°S, Easterlies: average 10 m easterly winds strength (counted positive westward) computed between 66 and 70°S.

observed in Comiso et al. (2017). Over the continent, no significant overall temperature trend was found. The EC-Earth driven hindcasts simulate a 2 m air warming trend over the Southern Ocean (0.30 K per decade on average, Table 2). All three of those simulations also produce a positive Antarctic 2 m air temperature trend, but with a larger inter-member variability (from 0.14 to 0.27 K per decade, Tab. 2) and with a lower robustness for the trend fit (for FC02, the significance test fails) compared to the trends over the ocean. This illustrates the large contribution of internal variability to pluri-decadal temperature trends over Antarctica, which is consistent with barely significant trends in observations there (Turner et al., 2016, 2020).

The spatial patterns of temperature trends are overall matching the spatial patterns seen for the sea ice change (Fig. 7 and 5). There is a warming trend over large parts of the Southern Ocean around West Antarctica and a cooling trend around East Antarctica, common to all simulations. The ERA-5 driven simulation also has no significant surface temperature trend over West Antarctica, whereas the area of cooling is much larger and the cooling is more intensive in the Southern Ocean around East Antarctica. In the EC-Earth driven hindcasts, the area of warming extends over large parts of West Antarctica itself, including the peninsula and the Ross Ice shelf, as well as the Weddell Sea, which has no significant trend in the ERA-5 driven hindcast.

The findings for temperature illustrate the connection between temperature and sea ice, as warmer temperatures coincide with less sea ice. This connection may however work both ways, with warmer air increasing sea ice melt, and with sea ice inhibiting latent heat flux from the ocean. It is therefore useful to also look at trends in wind and geopotential as the other potential drivers of temperature differences. In the FC00 ensemble member, there is a strong amplification of the Amundsen Sea Low (ASL, see Fig. 8), which explains the increasing trend in westerly winds just north of it which is not seen in the other simulations (Tab. 2). FC01 and especially FC02 as the other EC-Earth driven ensemble members simulate a shift of the ASL towards the Ross Sea (Fig. 8). This pattern offers an explanation for the much stronger decrease in sea ice concentration seen for the eastern Amundsen and western Ross seas around 165°W (Fig. 5) in FC01 and FC02 compared to FC00. In those two hindcasts, the areas with a stronger sea ice trend lie between areas of increased geopotential to the east and decreased geopotential to the west, which causes more frequent or more intense northerly winds for that area. Overall, the trends in

https://doi.org/10.5194/egusphere-2025-2889
Preprint. Discussion started: 15 August 2025

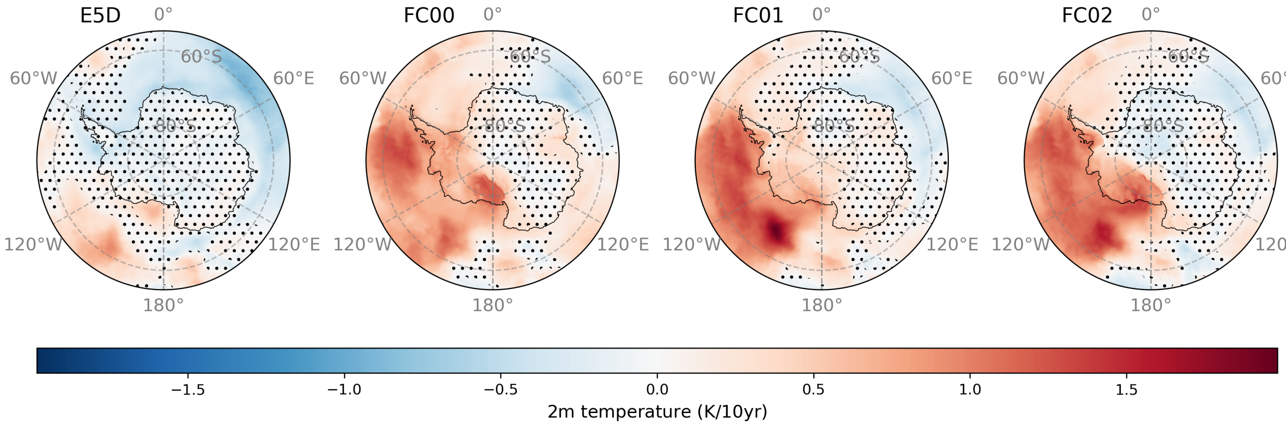

**Figure 7.** Yearly 2m temperature trends in different locations in Antarctica and the Southern Ocean for the ERA5-driven hindcast (E5D) and the three EC-Earth-driven hindcasts (FC00 – FC02). Hatched areas represent areas where the Mann-Kendall test does not reach a p-value of 0.05 or below.

the three EC-Earth driven hindcasts are much less consistent in the geopotential compared with those obtained for SIE and temperature. Finally, the ERA-5 driven hindcast shows signs of an intensification of the ASL, but at a much smaller scale than 330 FC00 and also not statistically significant (Fig. 8), while the geopotential in the Ross Sea does not seem to follow a particular pattern at all.

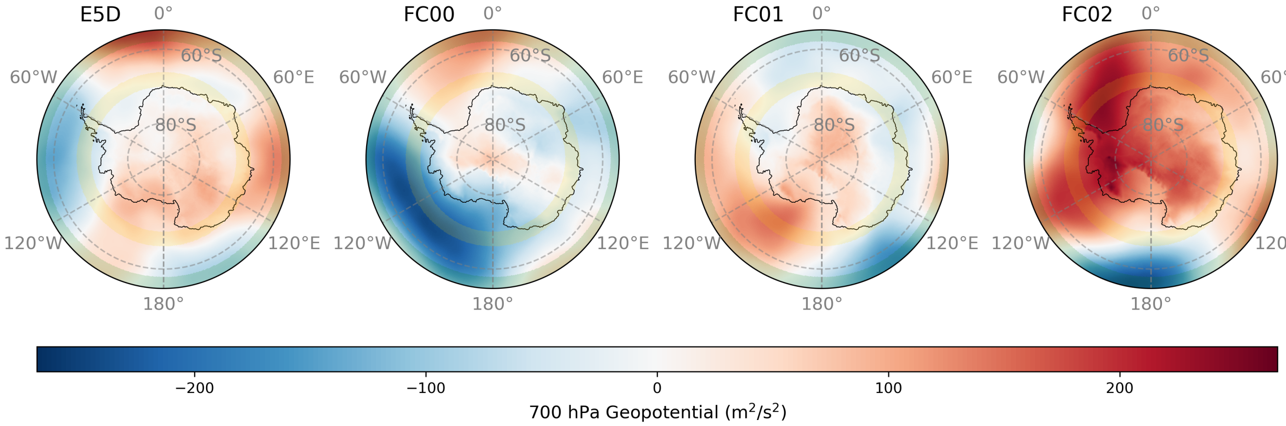

**Figure 8.** Average 850 hPa geopotential 2009–2014, compared to the 1985–1990 average, for the ERA5-driven hindcast (E5D) and the three EC-Earth-driven hindcasts (FC00 – FC02). The green stripe indicates the area for which in Tab. 2, the westerlies, and for the yellow stripe, the easterlies are calculated (Areas outside of the evaluation domain are not taken into account). Note that changes, instead of trends, are shown.

https://doi.org/10.5194/egusphere-2025-2889
Preprint. Discussion started: 15 August 2025

### 4.3 Evaporation, Precipitation, and Moisture Transport

| | **Prec. SO** | **Prec. AA** | **Evap. SO** | **MT boundary** | **MT AA** |
|---|---|---|---|---|---|
| | (Gt/yr/10yr) | (Gt/yr/10yr) | (Gt/yr/10yr) | (Gt/yr/10yr) | (Gt/yr/10yr) |
| E5D | 196.9 | -16.7* | -312.0 | 437.8 | -15.8* |
| FC00 | 565.2 | 89.1 | 295.1 | 348.9 | 82.6 |
| FC01 | 460.2 | 53.6 | 289.2 | 188.9 | 51.0* |
| FC02 | 453.1 | 87.9 | 355.0 | 171.1 | 83.0 |

**Table 3.** Decadal trends for moisture transport and precipitation computed over 1985-2014 for the ERA5-driven hindcast (E5D) and the three EC-Earth-driven hindcasts (FC00 – FC02). An asterisk indicates an insignificant trend ($p > 0.05$). All values in Gigatonnes per year per decade. MT: Moisture Transport, Prec: Precipitation, Evap.: Evaporation, boundary: at boundaries of the evaluation domain, SO: Southern Ocean, i.e. evaluation domain excluding landmasses, AA: Antarctica, i.e. landmasses south of 60° south. MT continent is equivalent to the surface mass balance of Antarctica.

With a lower overall air temperature, it is expected that precipitation decreases. This is because lower temperatures generally decrease the saturation water vapour pressure, which impedes both evaporation and moisture transport from the warmer mid-latitudes towards the continent. It is therefore surprising that the ERA-5 driven hindcast is simulating an increase in precipitation over the Southern Ocean of 196.9 Gt/yr per decade (Tab. 3), despite the decreases in temperature (Tab. 2). However, this surprising trend cannot be seen over the continent, where the precipitation trend is insignificant (Tab. 3), which is in line with the insignificant temperature trend (Tab. 2). The EC-Earth driven hindcasts simulate an increase in precipitation over the Southern Ocean of on average 492.8 Gt/yr per decade, which is more in line with our expectations, and two out of the three hindcasts also display a moderate increasing trend over the continent, consistent with the increase in temperature seen there.

Evaporation, which is one of the possible sources of moisture and thus precipitation, is more in line with the temperature trends. The ERA5 driven hindcast simulates a significant decrease in evaporation over the Southern Ocean of 312.0 Gt/yr per decade. In addition to the air temperature, the sea ice concentration also plays a role here as an insulating layer between the ocean and the atmosphere. Since sea ice concentration decreases in the EC-Earth driven hindcasts, it makes sense that evaporation is increasing significantly for all 3 ensemble members, with on average 313.1 Gt/yr per decade. The correlation of evaporation and sea ice concentration becomes even more apparent when looking at the spatial distribution of the trends. The ERA5 driven hindcast has indeed the strongest decrease in evaporation in the ocean around East Antarctica (Fig. 9), where also it simulated the largest increase in sea ice concentration (Fig. 5). Conversely, the EC-Earth driven hindcast is simulating its increases in evaporation predominantly in the Ross Sea, which is especially true for ensemble members FC01 and FC02 (which had a particularly strong sea ice concentration decrease there, see Fig. 5). It is also noteworthy that the areas of strong evaporation trends largely line up with the areas with a correspondingly strong precipitation trend, indicating that a sizeable part of an increased evaporation has a low residence time in the air and thus falls out as precipitation in the same area.

Apart from changing evaporation over the Southern Ocean, changing moisture transport into the model domain from the lateral boundaries is also a possible cause of trends in precipitation. For longer timescales, changing storage of moisture in the

https://doi.org/10.5194/egusphere-2025-2889
Preprint. Discussion started: 15 August 2025

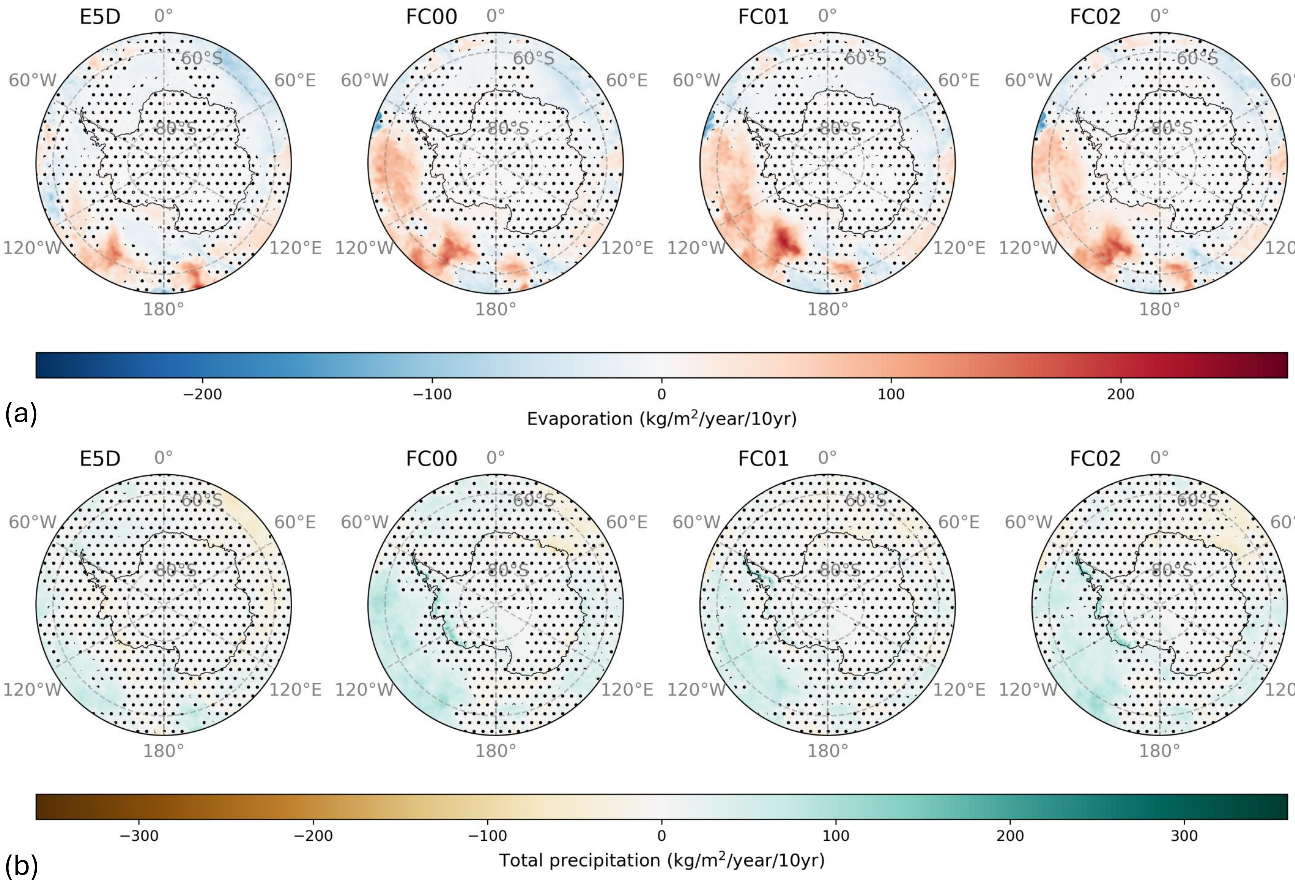

**Figure 9.** Evaporation (a) and precipitation (b) trends in different locations in Antarctica and the Southern Ocean for the ERA5-driven hindcast (E5D) and the three EC-Earth-driven hindcasts (FC00 – FC02). Hatched areas represent areas where the Mann-Kendall test does not reach a p-value of 0.05 or below.

atmosphere can be ignored, and moisture transport into an arbitrary domain is identical to precipitation minus evaporation over the area of interest (in this case, the evaluation domain except the South American continent, or later the Antarctic continent). After all, precipitation that does not have a local source has to have an origin somewhere else, and all evaporation that does not fall out as precipitation within the area of interest has to have been transported somewhere else. Given that in the ERA5 driven hindcast, precipitation over the Southern Ocean increased and remained the same over the Antarctic continent while evaporation decreased, it is not surprising that there is a strong increase in moisture transport into the evaluation domain of 437.8 Gt/yr per decade (Tab. 3), likely driving the increasing trend in precipitation. Very surprising is that this increase in moisture transport seemingly contradicts the decreasing trend in temperature (Fig. 6), as the colder air should only be able to transport a decreased amount of water. The increasing trend is therefore likely related to either an asymmetric temperature change for flow into and out of the domain, or changing atmospheric dynamics, but further analysis would be needed to verify this hypothesis. There

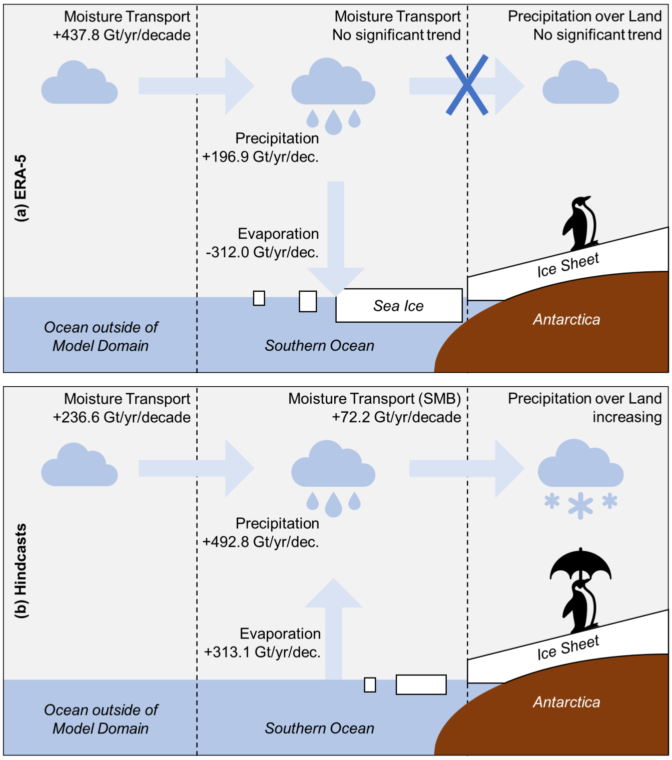

**Figure 10.** Changes in moisture fluxes. In both the ERA5 driven hindcast (a) and the EC-Earth driven hindcasts (b), the moisture transport from the model boundaries is significantly increasing, but in (b), Evaporation has a decreasing trend, presumably also due to the higher amount of sea ice. As a result, moisture flux and precipitation over the continent do not have an increasing trend in (b).

is no significant change in the moisture transport into the Antarctic continent for the ERA5 driven hindcast, indicating that the increase in moisture transport from the model boundaries doesn't reach the continent and falls out as precipitation earlier. In the EC-Earth driven hindcasts, the moisture transport into the evaluation domain is increasing, as would be expected from the increasing temperature. However, the increase amount varies strongly in between the ensemble members, ranging from 171.1 Gt/yr per decade in FC02 to 348.9 Gt/yr per decade in FC00 (Tab. 3). As the increase in moisture transport from the mid-latitudes and evaporation is larger than the increase in precipitation over the Southern Ocean, the remaining moisture has to be transported to the Antarctic continent, where indeed moisture transport is increasing by on average 72.2 Gt/yr per decade. It is possible that the decrease in sea ice concentration in the EC-Earth driven hindcasts plays an important role here, as a decrease in sea ice, which has evaporation-inhibiting properties, leads to more available moisture close to the continent. In contrast to that, sea ice concentration in the ERA5 driven hindcast increases (Tab. 1), which inhibits evaporation and therefore could prevent that moisture from reaching the continent. The increased moisture transport then falls out over the Southern Ocean and the sea ice, while not being compensated with more evaporation (Fig. 10).

### 4.4 Clouds

| | **SO IWP** ($10^{-5}$ kg/m$^2$/10yr) | **SO LWP** ($10^{-5}$ kg/m$^2$/10yr) | **SO CC** ($10^{-5}$ %/10yr) | **AA IWP** ($10^{-5}$ kg/m$^2$/10yr) | **AA LWP** ($10^{-5}$ kg/m$^2$/10yr) | **AA CC** ($10^{-5}$ %/10yr) |
|---|---|---|---|---|---|---|
| E5D | 1.94 | 60.5 | 1.23 | -1.03* | -0.004* | 1.44* |
| FC00 | 9.05* | 119 | -0.89 | 14.2 | 2.58 | 1.71* |
| FC01 | 5.33* | 93.7 | -0.93 | 4.73* | 3.62 | 1.23* |
| FC02 | 7.79* | 97.1 | -1.06 | 9.63* | 3.44 | 1.05* |

**Table 4.** Decadal trends in vertically integrated cloud ice (Ice Water Path, IWP), vertically integrated cloud liquid water (Liquid Water Path, LWP), and total cloud cover (CC) for the different simulations, separated into Southern Ocean (SO) and Antarctic continent (AA), for the ERA5-driven hindcast (E5D) and the three EC-Earth-driven hindcasts (FC00 – FC02). An asterisk indicates an insignificant trend ($p > 0.05$).

All simulations demonstrate an increase in vertically integrated liquid water content (Tab. 4), consistent with the increase in moisture transport from the mid-latitudes. In the EC-Earth driven hindcasts, the increases are consistently larger than in the ERA5 driven hindcast, possibly facilitated by the increasing trend in evaporation. Noticeably, the cloud cover is declining for the EC-Earth driven hindcasts while moisture content is increasing, indicating that there are fewer, but thicker clouds. There are no significant trends in vertically integrated ice water content, with the exception of a weak increase over the Antarctic continent in the EC-Earth driven ensemble member FC00 (Tab. 4). The ERA5 driven hindcast is also not simulating a significant change in the vertically integrated liquid water content over the continent, whereas all three EC-Earth driven hindcasts do simulate a significant trend, consistent with the increase in precipitation and moisture transport to the continent that is not seen in the ERA5 driven run (as discussed in the previous section). However, the trend seen over the continent is an order of magnitude smaller than the trends seen over the Southern Ocean.

There is a spatial pattern within these trends, which are generally stronger over areas with increasing temperature trends and decreasing or increasing sea ice concentration trends (Fig. A6). Surprisingly, the increase in liquid water around West Antarctica in the EC-Earth driven simulations is stronger closer to the continent. This is likely related to the seasonal cycle, as liquid water in clouds close to the continent is more prevalent during austral summer, when SIE is at its minimum, and therefore indicates that these increases are indeed related to the decreasing trend in March SIE which can be seen in the EC-Earth driven hindcasts (Fig. 4). Consequently, in the ERA5 driven hindcast, there is a decrease in cloud liquid water around East Antarctica, but further off the coast compared to the increasing areas described previously for the EC-Earth driven hindcasts. This decrease can also be spotted with a much lower magnitude and spatial extent in the same places in the hindcast driven simulations, and is therefore likely related to the change in maximum SIE in the winter.

## 5 Discussion

PARASO improves the representation of climatic processes in the Antarctic region. Compared to GCMs, this is thanks to its higher resolution and usage of parameterizations specific to Antarctica. Compared to (atmospheric) RCMs, this is thanks to its

https://doi.org/10.5194/egusphere-2025-2889
Preprint. Discussion started: 15 August 2025

more extensive coupling functionality. This can be seen particularly well in the ERA5 driven hindcast, with its sea ice extent trend closely matching observations. Furthermore, the SMB trend in the ERA5 driven hindcast is insignificant or slightly declining, which is in agreement with previous work (Mottram et al., 2020). The declining SIE trend cannot be seen in the EC-Earth driven hindcasts. As all hindcasts share the same model physics and only differ in their forcing at the boundaries and in their initial conditions, this is an indication for a strong influence of the mid-latitude boundary conditions on SIE. This conclusion is further strengthened by previous work using PARASO regarding SIE drivers (Mezzina et al., 2024). The cooling trend seen on the domain boundaries for the ERA5 driven hindcast is likely a reason for its increasing SIE, compared to the EC-Earth driven hindcasts. Another difference is that the ERA5 reanalysis data provides a higher resolution than the EC-Earth hindcasts for the boundary conditions, with mesoscale systems being better resolved with the 30 km grid of ERA5. This might also explain the differences in SMB trends, as the accumulation over Antarctica is mostly determined by meridional moisture fluxes carried by mesoscale systems (Dalaiden et al., 2020).

With the exception of westerly winds, all the long-term trends we looked at in this study diverge between the ERA5 and the EC-Earth driven simulations. This can be traced back to strong interconnections between the variables: The temperatures simulated at the model boundaries heavily influences the moisture transport into the domain, but also the evaporation within the domain. The moisture fluxes into and out of the atmosphere over the Southern Ocean in turn have strong impacts on moisture transport towards the continent as well as cloud formation and precipitation amounts over the ocean. This link of connections then continues via moisture over the continent, hydrometeor masses and precipitation, until SMB is reached. These trends can be seen as rather robust, as they agree in between the ensemble members and have a logical physical connection, however, the (interannual) variability in most of the related atmospheric variables is much larger than that of ocean-related variables such as SIE. This can be seen in the moisture transport (Table 3), where the transport trend at the boundary conditions has strong fluctuations between the EC-Earth driven simulations, and for the transport trend towards the continent, one of the ensemble members doesn't reach a significant level in the Mann-Kendall-Test (FC01, $p = 0.062$). This behaviour is likely due to strong interannual variability, as is expected for atmospheric quantities which generally behave more chaotic than oceanic quantities, due to the ocean's larger inertia. For a longer simulation period, the trends would therefore likely reach a better agreement. For models at the resolution used here, often single model realizations of 30 years are analyzed, which is rather short given the slow ocean variability and high interannual variability of the atmosphere. This makes it difficult to differentiate internal variability (which would persist in longer time series) from interannual variability (which would be smoothened out by longer time series). With our approach where we have three hindcasts driven by EC-Earth, we can better differentiate internal variability from interannual variability.

## 6 Conclusions

This study presents the first retrospective hindcasts of the Antarctic climate's past decades performed with a fully-coupled, circum-Antarctic ocean–sea ice–ice sheet–atmosphere–land model. The model was shown to reproduce an overall realistic mean state of the Antarctic climate. Overall, the simulated mean state presents minor differences with the ocean standalone

https://doi.org/10.5194/egusphere-2025-2889
Preprint. Discussion started: 15 August 2025

runs of (Pelletier et al., 2022, P22), illustrating the stability of the coupled model. More precisely, the ERA5 driven hindcast simulates a realistic SIE seasonal cycle, except for an underestimation of the summer sea ice extent by $2.63 \cdot 10^6$ km$^2$, inherited from standalone NEMO simulations, which is likely amplified by the atmospheric coupling (P22). The simulated vertical temperature and salinity profiles in the ocean compare well with the observations, even within coastal seas, likely made possible by the relatively high resolution. We demonstrated the importance of mid-latitude forcing by creating an ensemble forced with EC-Earth output and comparing it with the ERA5 driven hindcast.

We disentangled the respective roles of midlatitude forcing and internal variability in some of the multi-decadal trends affecting the surface Antarctic climate. A key result is that the PARASO model is able to reproduce the observed positive SIE trend when forced with realistic boundary conditions coming from ERA5 and ORAS5 reanalyses, demonstrating its added value compared to low-resolution GCMs. These mostly simulate a sea ice decrease over the past decades (Roach et al., 2020). When forced with boundary conditions from EC-Earth, PARASO simulates a negative SIE trend similar to global climate models (GCMs), indicating a central role of midlatitude forcing in dictating SIE decadal variability. Most long-term trends (2 m air temperature, westerly wind trends over the Southern Ocean, Antarctic SMB, moisture transport) simulated in the EC-Earth driven hindcasts are common to all three members, illustrating the weak contribution of internal variability on these timescales for these variables. This is especially true over the ocean, whereas the trends over the Antarctic continent for surface temperature and wind have a larger imprint of internal variability. The ERA5 driven and EC-Earth driven hindcasts simulate opposing trends for not only SIE, but also near-surface temperature, moisture transport into, and precipitation over Antarctica. The differences in moisture transport towards Antarctica and precipitation over Antarctica can be explained by the increasing SIE, which limits evaporation close to Antarctica in the case of the ERA5 driven hindcast. In the case of the EC-Earth driven hindcasts, the decrease in SIE seems to be driven in part by a much stronger intensification of the Amundsen Sea Low compared to the ERA5 driven hindcast as well as a shifted location, increasing northerly winds between the Ross and Amundsen Seas and thus causing a stronger influx of moisture and heat.

Approaches based on such a regional coupled model open many opportunities to better understand the variability of the Antarctic climate. Our analysis highlights a strong sensitivity of climatic trends in Antarctica and the Southern Ocean to mid-latitude processes. This sensitivity should be explored in more detail, in order to better understand which trends are directly linked to the change in forcing, and which are downstream effects of other trends. Finally, downscaling future climate simulations produced with GCMs using PARASO would allow a more confident projection of the way global warming will affect the Antarctic climate.

## Appendix A: Appendix

The vertical distributions of water temperature and salinity are well captured by both EC-Earth driven and ERA5 driven experiments (Figure A3), although a potential drift in deep ocean would still need a longer simulation period to become apparent. There is a warm bias in the upper ocean in the Western Pacific sector of approximately 1°C (Fig. A3 f), and there are

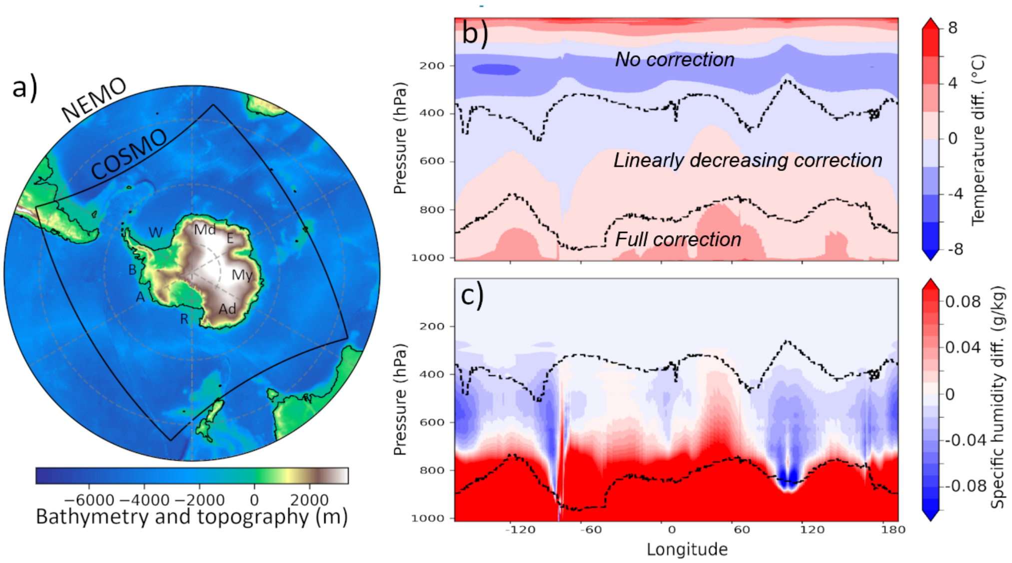

**Figure A1.** a) Bathymetry and topography map with boundaries of the COSMO (black square) and NEMO (outer black circle) domains, A: Amundsen Sea, B: Bellingshausen Sea, W: Weddell Sea, Md: Queen Maud Land, E: Enderby Land, My: Queen Mary Land, Ad: Adélie Land, R: Ross Sea. b) vertical profiles of annual mean temperature and c) specific humidity differences between the EC-Earth and ERA5 1985-2014 climatology, taken along the COSMO boundary. The dashed black lines represent the limits of the bias correction application: full correction below the first (from the ground) line, linearly decreasing bias correction between the first and second line, no correction above the second line.

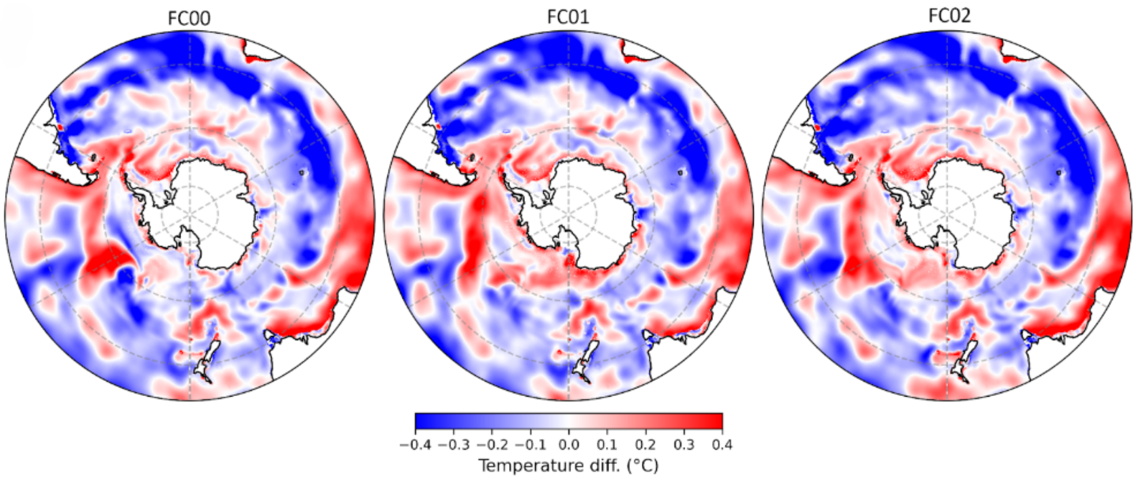

**Figure A2.** 0-1000 m average ocean temperature anomalies of January 1985 of ORAS4 which are added to the ocean standalone climatology to produce the initial states of the three EC-Earth-driven hindcasts.

cold biases in the Bellingshausen and Amundsen sectors (Fig. A3b and c) for both the EC-Earth driven ensemble and for the ERA5-driven hindcast. These cold biases amount to 1°C (EC-Earth) and 2°C (ERA5) in the upper 100 m of the open ocean and 1 to 2°C cold biases below 250 m underneath the ice shelf. This cold bias makes these sectors more resembling of the cold coastal seas of East Antarctica than the observed warm coastal seas typical of West Antarctica (as shown by the climatology in 470 Fig. A3b and A3c, see also Locarnini et al. (2018). Near-surface salinity is well-captured by the model, with the exception of a fresh bias mostly visible in the Weddell Sea and in the coastal seas of the Indian sector. There is also a marked fresh bias (-0.25 psu to -0.5 psu) in the subsurface (below 250) in all sectors. Here again, those biases are independent of the forcing used. It can finally be noted that the three EC-Earth-driven hindcasts simulate identical mean vertical profiles, with the exception of the first 50 m of the open ocean in the Bellingshausen Sea.

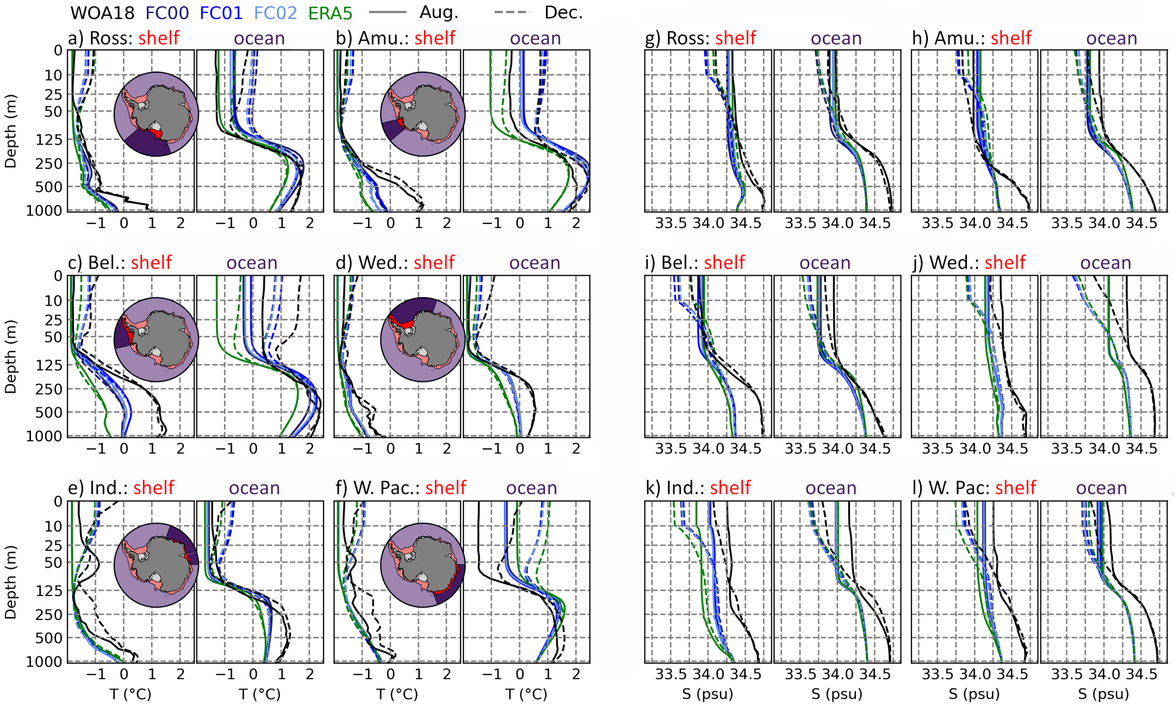

**Figure A3.** Vertical profiles of ocean temperature (left) and salinity (right) observed in the WOA18 climatology (Locarnini et al., 2018) and simulated in the 4 PARASO hindcasts (1985-2014 average), for the open ocean (dark purple) and coastal seas (red) of each sector of Antarctica. Winter: solid line, Summer (dashed line). WOA18 is represented in black, the three EC-Earth-driven hindcasts in blue, and the ERA5-driven run in green. Note the non-linearity of the vertical axis. Amu.: Amundsen, Bel.: Bellingshausen, Wed.: Weddell, Ind: Indian sector, W. Pac.: west Pacific.

475 The mean basal ice shelf melts simulated by the four PARASO hindcasts are compared to observational estimates in Figure A5. For the Ross Sea, Weddell Sea, and Indian Ocean sectors, the simulated basal melts compare well with the estimates of Rignot et al. (2013) and Adusumilli et al. (2020). In the Western Pacific sector, and more importantly in the Bellingshausen

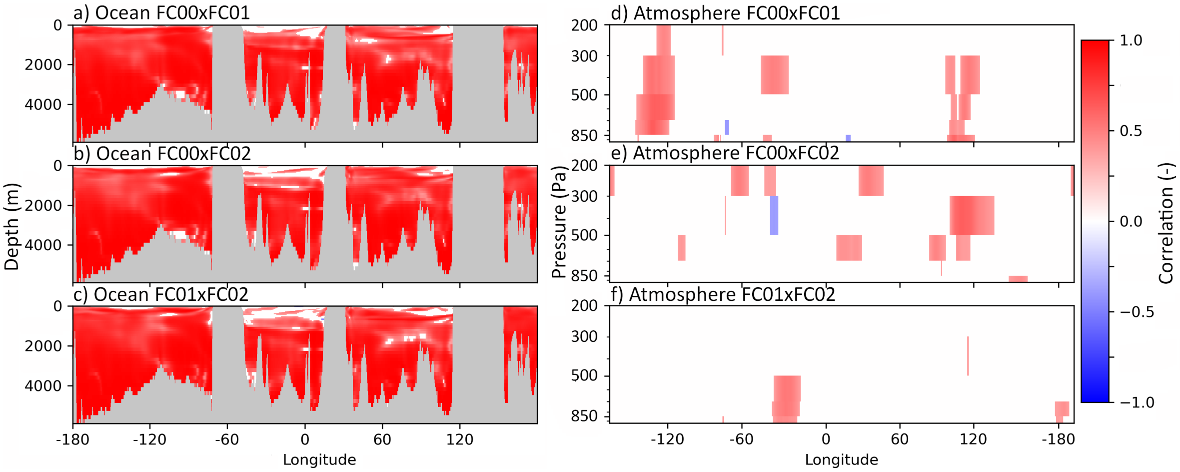

**Figure A4.** Vertical profiles of yearly ocean temperature anomalies (a, b, and c) and atmosphere temperature anomalies (d, e, and f) cross-member correlations (a, d: FC00 with FC01, b, e: FC00 and FC02, c, f: FC01 with FC02) taken along each model lateral boundary (see Figure A1a). Yearly temperature anomalies time series were linearly detrended before computing the correlation. Only statistically significant ($p < 0.05$) correlations are shown.

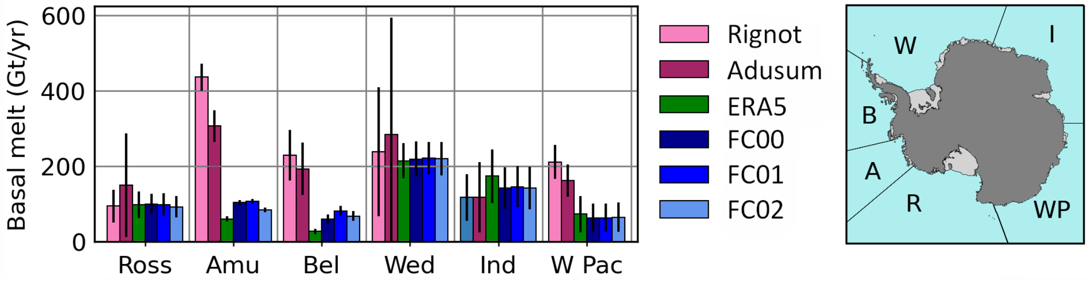

**Figure A5.** Mean sector-wide ice shelves basal melt estimated by Rignot et al. (2013) and Adusumilli et al. (2020), and simulated in the EC-Earth-driven and ERA5-driven hindcasts. Sector names: R = Ross, A = Amundsen, B = Bellingshausen, W = Weddell, I = Indian, WP = West Pacific.

and Amundsen Seas, the four PARASO hindcasts underestimate ice shelf basal melt with mean biases of respectively -138 (-148), -202 (-159), -376 (-338) Gt/yr for the ERA5-driven run (resp., for the EC-Earth-driven runs ensemble mean). These negative biases seem to be independent of the forcing used since they are found in both the ERA5/ORAS5-driven run and in the EC-Earth-driven runs. The underestimation of basal melt in the Amundsen and Bellinghsausen Seas can be traced back to the colder than observed ocean temperature there, suggesting an oceanic origin rather than a tuning or ice shelf geometry representation issue.

https://doi.org/10.5194/egusphere-2025-2889
Preprint. Discussion started: 15 August 2025

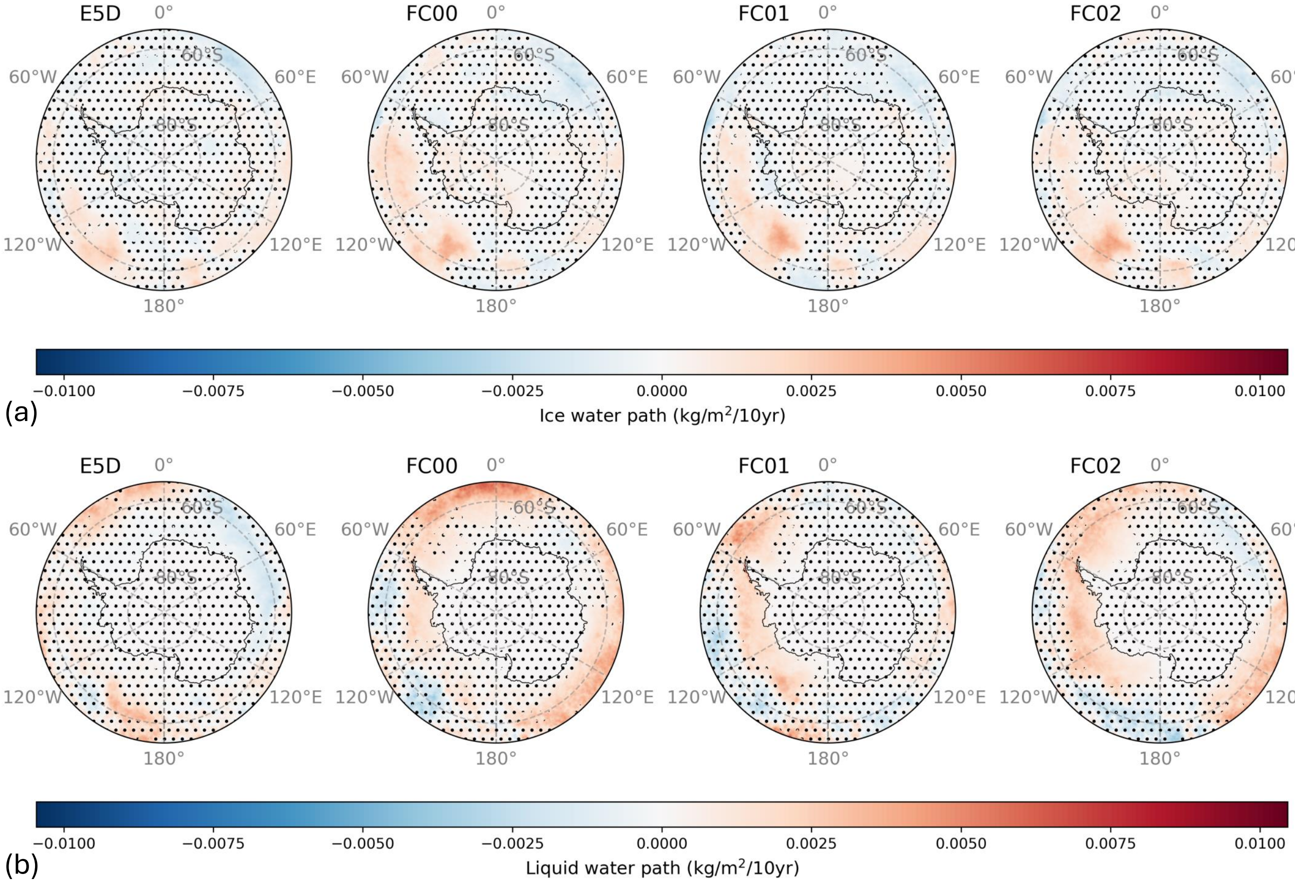

**Figure A6.** Cloud ice (a) and water (b) trends in different locations in Antarctica and the Southern Ocean for the ERA5-driven hindcast (E5D) and the three EC-Earth-driven hindcasts (FC00 – FC02). Hatched areas represent areas where the Mann-Kendall test does not reach a p-value of 0.05 or below.

*Author contributions.* This study was conceptualised by PVH, FS, NvL, TF, and HG. The PARASO hindcasts presented in this run and the corresponding code were produced and maintained by PVH and SM. Funding was acquired by TF, FP, HG, and NvL. The project was planned and supervised by FP, HG, and NvL. Additional software development was done by EMC, FP, FK. The model output was investigated and formally analyzed by FS, PVH, LZ, EMC, SM, and DV. The methodology was developed by PVH, FS, BM, FM, EMC, CP, TP, FP, LZ, HG, PO, FK, KH, SM, and NvL. Model output was validated by FS, PVH, TF, and KH; and visualised by FS and PVH. The original manuscript drafts were written by FS and PVH, and reviewed by NvL, BM, CP, TF, HG, PO, KH, and DV.

*Competing interests.* The authors declare that they have no competing interests.

*Acknowledgements.* This work was financially supported by the PARAMOUR project, Decadal predictability and variability of polar climate: the role of atmosphere-ocean-cryosphere multiscale interactions, supported by the Fonds de la Recherche Scientifique–FNRS under Grant number O0100718F (EOS ID 30454083); and by the Belgian Science Policy Office (BELSPO) through project no. RT/23/PASPARTOUT (PASPARTOUT - Pathways of particles, VOCs and moisture into East-Antarctica in a changing climate) as part of its IMPULS programme. The computational resources and services used in this work were provided by: the VSC (Flemish Supercomputer Center), funded by the Research Foundation - Flanders (FWO) and the Flemish Government; the supercomputing facilities of the Université Catholique de Louvain (CISM/UCL) and the Consortium des Équipements de Calcul Intensif en Fédération Wallonie Bruxelles (CÉCI) funded by the Fond de la Recherche Scientifique de Belgique (F.R.S.-FNRS) under convention 2.5020.11 and by the Walloon Region. The ERA5 data Hersbach et al. (2020) was downloaded on 01-SEP-2019 from the Copernicus Climate Change Service (C3S) Climate Data Store. The results contain modified Copernicus Climate Change Service information 2020. Neither the European Commission nor ECMWF is responsible for any use that may be made of the Copernicus information or data it contains.

## References

Adusumilli, S., Fricker, H. A., Medley, B., Padman, L., and Siegfried, M. R.: Interannual variations in meltwater input to the Southern Ocean from Antarctic ice shelves, Nature Geoscience, 13, 616–620, 2020.

Barrand, N. E., Vaughan, D. G., Steiner, N., Tedesco, M., Kuipers Munneke, P., van den Broeke, M. R., and Hosking, J. S.: Trends in Antarctic Peninsula surface melting conditions from observations and regional climate modeling, Journal of Geophysical Research: Earth Surface, 118, 315–330, https://doi.org/https://doi.org/10.1029/2012JF002559, 2013.

Barthélemy, A., Goosse, H., Fichefet, T., and Lecomte, O.: On the sensitivity of Antarctic sea ice model biases to atmospheric forcing uncertainties, Clim. Dyn., 51, 1585–1603, https://doi.org/10.1007/s00382-017-3972-7, 2018.

Bilbao, R., Wild, S., Ortega, P., Acosta-Navarro, J., Arsouze, T., Bretonnière, P.-A., Caron, L.-P., Castrillo, M., Cruz-García, R., Cvijanovic, I., Doblas-Reyes, F. J., Donat, M., Dutra, E., Echevarría, P., Ho, A.-C., Loosveldt-Tomas, S., Moreno-Chamarro, E., Pérez-Zanon, N., Ramos, A., Ruprich-Robert, Y., Sicardi, V., Tourigny, E., and Vegas-Regidor, J.: Assessment of a full-field initialized decadal climate prediction system with the CMIP6 version of EC-Earth, Earth System Dynamics, 12, 173–196, https://doi.org/10.5194/esd-12-173-2021, publisher: Copernicus GmbH, 2021.

Comiso, J. C., Meier, W. N., and Gersten, R.: Variability and trends in the Arctic Sea ice cover: Results from different techniques, Journal of Geophysical Research: Oceans, 122, 6883–6900, https://doi.org/10.1002/2017JC012768, _eprint: https://onlinelibrary.wiley.com/doi/pdf/10.1002/2017JC012768, 2017.

Coulon, V., Bulthuis, K., Whitehouse, P. L., Sun, S., Haubner, K., Zipf, L., and Pattyn, F.: Contrasting Response of West and East Antarctic Ice Sheets to Glacial Isostatic Adjustment, J. Geophys. Res. Earth Surf., 126, e2020JF006 003, https://doi.org/10.1029/2020JF006003, 2021.

Dalaiden, Q., Goosse, H., Lenaerts, J. T. M., Cavitte, M. G. P., and Henderson, N.: Future Antarctic snow accumulation trend is dominated by atmospheric synoptic-scale events, Communications Earth & Environment, 1, 62, https://doi.org/10.1038/s43247-020-00062-x, 2020.

Dalaiden, Q., Schurer, A. P., Kirchmeier-Young, M. C., Goosse, H., and Hegerl, G. C.: West Antarctic Surface Climate Changes Since the Mid-20th Century Driven by Anthropogenic Forcing, Geophysical Research Letters, 49, e2022GL099 543, https://doi.org/https://doi.org/10.1029/2022GL099543, e2022GL099543 2022GL099543, 2022.

De Lavergne, C., Palter, J. B., Galbraith, E. D., Bernardello, R., and Marinov, I.: Cessation of deep convection in the open Southern Ocean under anthropogenic climate change, Nature Climate Change, 4, 278, 2014.

Donat-Magnin, M., Jourdain, N. C., Spence, P., Le Sommer, J., Gallée, H., and Durand, G.: Ice-Shelf Melt Response to Changing Winds and Glacier Dynamics in the Amundsen Sea Sector, Antarctica, Journal of Geophysical Research: Oceans, 122, 10 206–10 224, 2017.

Döscher, R., Acosta, M., Alessandri, A., Anthoni, P., Arneth, A., Arsouze, T., Bergmann, T., Bernadello, R., Bousetta, S., Caron, L.-P., Carver, G., Castrillo, M., Catalano, F., Cvijanovic, I., Davini, P., Dekker, E., Doblas-Reyes, F. J., Docquier, D., Echevarria, P., Fladrich, U., Fuentes-Franco, R., Gröger, M., v. Hardenberg, J., Hieronymus, J., Karami, M. P., Keskinen, J.-P., Koenigk, T., Makkonen, R., Massonnet, F., Ménégoz, M., Miller, P. A., Moreno-Chamarro, E., Nieradzik, L., van Noije, T., Nolan, P., O'Donnell, D., Ollinaho, P., van den Oord, G., Ortega, P., Prims, O. T., Ramos, A., Reerink, T., Rousset, C., Ruprich-Robert, Y., Le Sager, P., Schmith, T., Schrödner, R., Serva, F., Sicardi, V., Sloth Madsen, M., Smith, B., Tian, T., Tourigny, E., Uotila, P., Vancoppenolle, M., Wang, S., Wårlind, D., Willén, U., Wyser, K., Yang, S., Yepes-Arbós, X., and Zhang, Q.: The EC-Earth3 Earth System Model for the Climate ModelIntercomparison Project 6, preprint, Climate and Earth system modeling, https://doi.org/10.5194/gmd-2020-446, 2021.

Döscher, R., Acosta, M., Alessandri, A., Anthoni, P., Arsouze, T., Bergman, T., Bernardello, R., Boussetta, S., Caron, L.-P., Carver, G., Castrillo, M., Catalano, F., Cvijanovic, I., Davini, P., Dekker, E., Doblas-Reyes, F. J., Docquier, D., Echevarria, P., Fladrich, U., Fuentes-Franco, R., Gröger, M., v. Hardenberg, J., Hieronymus, J., Karami, M. P., Keskinen, J.-P., Koenigk, T., Makkonen, R., Massonnet, F., Ménégoz, M., Miller, P. A., Moreno-Chamarro, E., Nieradzik, L., van Noije, T., Nolan, P., O'Donnell, D., Ollinaho, P., van den Oord, G., Ortega, P., Prims, O. T., Ramos, A., Reerink, T., Rousset, C., Ruprich-Robert, Y., Le Sager, P., Schmith, T., Schrödner, R., Serva, F., Sicardi, V., Sloth Madsen, M., Smith, B., Tian, T., Tourigny, E., Uotila, P., Vancoppenolle, M., Wang, S., Wårlind, D., Willén, U., Wyser, K., Yang, S., Yepes-Arbós, X., and Zhang, Q.: The EC-Earth3 Earth system model for the Coupled Model Intercomparison Project 6, Geoscientific Model Development, 15, 2973–3020, https://doi.org/10.5194/gmd-15-2973-2022, publisher: Copernicus GmbH, 2022.

EUMETSAT: Global sea ice concentration reprocessing data- set 1978-2015 (v1.2), 2015.

Eyring, V., Bony, S., Meehl, G. A., Senior, C. A., Stevens, B., Stouffer, R. J., and Taylor, K. E.: Overview of the Coupled Model Intercomparison Project Phase 6 (CMIP6) experimental design and organization, Geosci. Model Dev., 9, 1937–1958, https://doi.org/10.5194/gmd-9-1937-2016, 2016.

Favier, L., Durand, G., Cornford, S. L., Gudmundsson, G. H., Gagliardini, O., Gillet-Chaulet, F., Zwinger, T., Payne, A. J., and Le Brocq, A. M.: Retreat of Pine Island Glacier controlled by marine ice-sheet instability, Nature Climate Change, 4, 117–121, https://doi.org/10.1038/nclimate2094, bandiera_abtest: a Cg_type: Nature Research Journals Number: 2 Primary_atype: Research Publisher: Nature Publishing Group Subject_term: Climate change;Cryospheric science;Environmental sciences Subject_term_id: climate-change;cryospheric-science;environmental-sciences, 2014.

Goosse, H., Kay, J. E., Armour, K. C., Bodas-Salcedo, A., Chepfer, H., Docquier, D., Jonko, A., Kushner, P. J., Lecomte, O., Massonnet, F., Park, H.-S., Pithan, F., Svensson, G., and Vancoppenolle, M.: Quantifying climate feedbacks in polar regions, Nature Communications, 9, 1919, https://doi.org/10.1038/s41467-018-04173-0, 2018.

Hersbach, H., Bell, B., Berrisford, P., Hirahara, S., Horányi, A., Muñoz-Sabater, J., Nicolas, J., Peubey, C., Radu, R., Schepers, D., and others: The ERA5 global reanalysis, Quarterly Journal of the Royal Meteorological Society, 146, 1999–2049, 2020.

Heuzé, C.: Antarctic Bottom Water and North Atlantic Deep Water in CMIP6 models, Ocean Science, 17, 59–90, https://doi.org/10.5194/os-17-59-2021, publisher: Copernicus GmbH, 2021.

Holmes, C. R., Bracegirdle, T. J., Holland, P. R., Stroeve, J., and Wilkinson, J.: Brief communication: New perspectives on the skill of modelled sea ice trends in light of recent Antarctic sea ice loss, The Cryosphere, 18, 5641–5652, https://doi.org/10.5194/tc-18-5641-2024, 2024.

Huot, P.-V., Kittel, C., Fichefet, T., Jourdain, N. C., Sterlin, J., and Fettweis, X.: Effects of the atmospheric forcing resolution on simulated sea ice and polynyas off Adélie Land, East Antarctica, Ocean Modelling, 168, 101 901, https://doi.org/10.1016/j.ocemod.2021.101901, 2021.

Jones, M. E., Bromwich, D. H., Nicolas, J. P., Carrasco, J., Plavcová, E., Zou, X., and Wang, S.-H.: Sixty Years of Widespread Warming in the Southern Middle and High Latitudes (1957–2016), Journal of Climate, 32, 6875–6898, https://doi.org/10.1175/JCLI-D-18-0565.1, publisher: American Meteorological Society Section: Journal of Climate, 2019.

Kittel, C., Amory, C., Agosta, C., Jourdain, N. C., Hofer, S., Delhasse, A., Doutreloup, S., Huot, P.-V., Lang, C., and Fichefet, T.: Diverging future surface mass balance between the Antarctic ice shelves and grounded ice sheet, The Cryosphere, 15, 1215–1236, publisher: Copernicus GmbH, 2021.

Kröger, J., Pohlmann, H., Sienz, F., Marotzke, J., Baehr, J., Köhl, A., Modali, K., Polkova, I., Stammer, D., Vamborg, F. S. E., and Müller, W. A.: Full-field initialized decadal predictions with the MPI earth system model: an initial shock in the North Atlantic, Climate Dynamics, 51, 2593–2608, https://doi.org/10.1007/s00382-017-4030-1, 2018.

Locarnini, R., Mishonov, A., Baranova, O., Boyer, T., Zweng, M., Garcia, H., Reagan, J., Seidov, D., Weathers, K., Paver, C., and Smolyar, I.: World Ocean Atlas 2018, Volume 1: Temperature, NOAA Atlas NESDIS 81, edition: A. Mishonov, 2018.

Madec, G.: NEMO ocean engine, Note du Pôle de modélisation, Institut Pierre-Simon Laplace (IPSL), France, No 27, ISSN No 1288-1619, 2016.

Mathiot, P., Jenkins, A., Harris, C., and Madec, G.: Explicit representation and parametrised impacts of under ice shelf seas in the z* coordinate ocean model NEMO 3.6, Geoscientific Model Development, 10, 2849–2874, https://doi.org/10.5194/gmd-10-2849-2017, 2017.

Mezzina, B., Goosse, H., Huot, P.-V., Marchi, S., and Van Lipzig, N.: Contributions of atmospheric forcing and ocean preconditioning in the 2016 Antarctic sea ice extent drop, Environmental Research: Climate, 3, 021 002, https://doi.org/10.1088/2752-5295/ad3a0b, 2024.

Mottram, R., Hansen, N., Kittel, C., van Wessem, M., Agosta, C., Amory, C., Boberg, F., van de Berg, W. J., Fettweis, X., Gossart, A., and others: What is the surface mass balance of Antarctica? An intercomparison of regional climate model estimates, The Cryosphere Discussions, pp. 1–42, 2020.

Oleson, K. W., Lawrence, D. M., Bonan, G. B., Drewniak, B., Huang, M., Koven, C. D., Levis, S., Li, F., Riley, W. J., Subin, Z. M., Swenson, S. C., Thornton, P. E., Bozbiyik, A., Fisher, R., Heald, C. L., Kluzek, E., Lamarque, J.-F., Lawrence, P. J., Leung, L. R., Lipscomb, W., Muszala, S., Ricciuto, D. M., Sacks, W., Sun, Y., Tang, J., and Yang, Z.-L.: Technical Description of version 4.5 of the Community Land Model (CLM), Tech. Rep. July, NCAR, http://www.cesm.ucar.edu/models/cesm1.2/clm/CLM45_Tech_Note.pdf, 2013.

Parkinson, C. L.: A 40-y record reveals gradual Antarctic sea ice increases followed by decreases at rates far exceeding the rates seen in the Arctic, Proceedings of the National Academy of Sciences, 116, 14 414–14 423, https://doi.org/10.1073/pnas.1906556116, publisher: Proceedings of the National Academy of Sciences, 2019.

Pattyn, F.: Sea-level response to melting of Antarctic ice shelves on multi-centennial timescales with the fast Elementary Thermomechanical Ice Sheet model (f.ETISh v1.0), Cryosphere, 11, 1851–1878, https://doi.org/10.5194/tc-11-1851-2017, 2017.

Pelletier, C., Fichefet, T., Goosse, H., Haubner, K., Helsen, S., Huot, P.-V., Kittel, C., Klein, F., Le clec'h, S., van Lipzig, N. P. M., Marchi, S., Massonnet, F., Mathiot, P., Moravveji, E., Moreno-Chamarro, E., Ortega, P., Pattyn, F., Souverijns, N., Van Achter, G., Vanden Broucke, S., Vanhulle, A., Verfaillie, D., and Zipf, L.: PARASO, a circum-Antarctic fully coupled ice-sheet–ocean–sea-ice–atmosphere–land model involving f.ETISh1.7, NEMO3.6, LIM3.6, COSMO5.0 and CLM4.5, Geoscientific Model Development, 15, 553–594, https://doi.org/10.5194/gmd-15-553-2022, publisher: Copernicus GmbH, 2022.

Rantanen, M., Karpechko, A. Y., Lipponen, A., Nordling, K., Hyvärinen, O., Ruosteenoja, K., Vihma, T., and Laaksonen, A.: The Arctic has warmed nearly four times faster than the globe since 1979, Communications Earth & Environment, 3, 1–10, https://doi.org/10.1038/s43247-022-00498-3, number: 1 Publisher: Nature Publishing Group, 2022.

Rignot, E., Jacobs, S., Mouginot, J., and Scheuchl, B.: Ice-Shelf Melting Around Antarctica, Science, 341, 266–270, https://doi.org/10.1126/science.1235798, 2013.

Roach, L. A., Dörr, J., Holmes, C. R., Massonnet, F., Blockley, E. W., Notz, D., Rackow, T., Raphael, M. N., O'Farrell, S. P., Bailey, D. A., and Bitz, C. M.: Antarctic Sea Ice Area in CMIP6, Geophysical Research Letters, 47, e2019GL086 729, https://doi.org/10.1029/2019GL086729, _eprint: https://agupubs.onlinelibrary.wiley.com/doi/pdf/10.1029/2019GL086729, 2020.

Rockel, B., Will, A., and Hense, A.: The Regional Climate Model COSMO-CLM (CCLM), Meteorologische Zeitschrift, 17, 347–348, https://doi.org/10.1127/0941-2948/2008/0309, 2008.

Rousset, C., Vancoppenolle, M., Madec, G., Fichefet, T., Flavoni, S., Barthélemy, A., Benshila, R., Chanut, J., Levy, C., Masson, S., and Vivier, F.: The Louvain-La-Neuve sea ice model LIM3.6: global and regional capabilities, Geoscientific Model Development, 8, 2991–3005, https://doi.org/10.5194/gmd-8-2991-2015, 2015.

Singh, H. A., Polvani, L. M., and Rasch, P. J.: Antarctic Sea Ice Expansion, Driven by Internal Variability, in the Presence of Increasing Atmospheric CO2, Geophysical Research Letters, 46, 14 762–14 771, https://doi.org/10.1029/2019GL083758, _eprint: https://onlinelibrary.wiley.com/doi/pdf/10.1029/2019GL083758, 2019.

Smith, R. S., Mathiot, P., Siahaan, A., Lee, V., Cornford, S. L., Gregory, J. M., Payne, A. J., Jenkins, A., Holland, P. R., Ridley, J. K., and Jones, C. G.: Coupling the U.K. Earth System Model to Dynamic Models of the Greenland and Antarctic Ice Sheets, J. Adv. Model. Earth Syst., 13, e2021MS002 520, https://doi.org/10.1029/2021MS002520, 2021.

Souverijns, N., Gossart, A., Demuzere, M., Lenaerts, J. T. M., Medley, B., Gorodetskaya, I. V., Vanden Broucke, S., and van Lipzig, N. P. M.: A New Regional Climate Model for POLAR-CORDEX: Evaluation of a 30-Year Hindcast with COSMO-CLM2 Over Antarctica, J. Geophys. Res. Atmos., 124, 1405–1427, https://doi.org/10.1029/2018JD028862, 2019.

Storkey, D., Blaker, A. T., Mathiot, P., Megann, A., Aksenov, Y., Blockley, E. W., Calvert, D., Graham, T., Hewitt, H. T., Hyder, P., and others: UK Global Ocean GO6 and GO7: A traceable hierarchy of model resolutions, Geoscientific Model Development, 11, 3187–3213, 2018.

Turner, J., Hosking, J. S., Bracegirdle, T. J., Marshall, G. J., and Phillips, T.: Recent changes in Antarctic sea ice, Philosophical Transactions of the Royal Society A: Mathematical, Physical and Engineering Sciences, 373, 20140 163, 2015.

Turner, J., Lu, H., White, I., King, J. C., Phillips, T., Hosking, J. S., Bracegirdle, T. J., Marshall, G. J., Mulvaney, R., and Deb, P.: Absence of 21st century warming on Antarctic Peninsula consistent with natural variability, Nature, 535, 411–415, https://doi.org/10.1038/nature18645, number: 7612 Publisher: Nature Publishing Group, 2016.

Turner, J., Marshall, G. J., Clem, K., Colwell, S., Phillips, T., and Lu, H.: Antarctic temperature variability and change from station data, International Journal of Climatology, 40, 2986–3007, https://doi.org/10.1002/joc.6378, _eprint: https://onlinelibrary.wiley.com/doi/pdf/10.1002/joc.6378, 2020.

Valcke, S.: The OASIS3 coupler: a European climate modelling community software, Geoscientific Model Development, 6, 373–388, https://doi.org/10.5194/gmd-6-373-2013, publisher: Copernicus GmbH, 2013.

Vancoppenolle, M., Fichefet, T., Goosse, H., Bouillon, S., Madec, G., and Maqueda, M. A. M.: Simulating the mass balance and salinity of Arctic and Antarctic sea ice. 1. Model description and validation, Ocean Modelling, 27, 33–53, https://doi.org/10.1016/j.ocemod.2008.10.005, 2009.

Volpi, D., Guemas, V., and Doblas-Reyes, F. J.: Comparison of full field and anomaly initialisation for decadal climate prediction: towards an optimal consistency between the ocean and sea-ice anomaly initialisation state, Climate Dynamics, 49, 1181–1195, https://doi.org/10.1007/s00382-016-3373-3, 2017.

Wang, Y., Zhou, D., Bunde, A., and Havlin, S.: Testing reanalysis data sets in Antarctica: Trends, persistence properties, and trend significance, Journal of Geophysical Research: Atmospheres, 121, 12,839–12,855, https://doi.org/10.1002/2016JD024864, _eprint: https://onlinelibrary.wiley.com/doi/pdf/10.1002/2016JD024864, 2016.

Yuan, N., Ding, M., Ludescher, J., and Bunde, A.: Increase of the Antarctic Sea Ice Extent is highly significant only in the Ross Sea, Scientific Reports, 7, 41 096, https://doi.org/10.1038/srep41096, number: 1 Publisher: Nature Publishing Group, 2017.

Zuo, H., Balmaseda, M. A., Tietsche, S., Mogensen, K., and Mayer, M.: The ECMWF operational ensemble reanalysis–analysis system for ocean and sea ice: a description of the system and assessment, Ocean Sci., 15, 779–808, https://doi.org/10.5194/os-15-779-2019, 2019.